The Combined Influence of Polythiophene Side Chains and Electrolyte Anions on Organic Electrochemical Transistors

Justine Wagner, Yunjia Song, Taein Lee, and Howard E. Katz
Department of Materials Science and Engineering, Johns Hopkins University, 206 Maryland Hall, 3400 North Charles Street, Baltimore, MD 21218

Abstract. Polythiophenes with differently functionalized side chains (alkyl, oligoethylene oxide, ester, hydroxy, and carboxylic acid) and varied counterions of potassium salt electrolytes were investigated in organic electrochemical transistors (OECTs). In addition, mixed blends were investigated to evaluate any synergistic effects between functionalities. Depending on the functional moiety attached, a large shift to lower potentials of V_{th}, an increase in drain current, and increase in transconductance can be observed compared to the base combination of alkyl side chain and Cl^-. The newly designed and synthesized hydroxy polymer displayed stability to large shifts in V_{TH}, slight increase in drain current, and little or no increase in transconductance when an ionic radius of the dopant is increased until a much larger anion, large polarizability, and low hydration number such as $TSFI^-$ was used. The acid-functionalized polymer, on the other hand had the same magnitude in shift with respect to any anion that is larger than Cl^-. The polymers were characterized by spectroscopy, x-ray diffraction, thermal analysis, and cyclic voltammetry. This work demonstrates that side-chain engineering can have substantial difference in the level of interaction in the electrolyte which would require tailoring the ion for specific polymer interactions.

Keywords. Polythiophenes, organic electrochemical transistors, transconductance, volumetric capacitance

1 Introduction

Conjugated polymers (CPs) have been a major focus of organic electronics[1-4] due to their potentially low cost, solution processability, and the possibility of synthetic design to generate desired electronic, optical, and mechanical functionality. CPs contribute to the activity of organic light-emitting diodes[4-8], organic thin film transistors[9-12], and organic photovoltaics[13-16]. More recently, conjugated polymers have also been used in electrochemical systems[17-18] that require polymers to simultaneously have both ionic and electronic charge density and conductivity, especially for bioelectronics that generally operate in aqueous media. This is extremely beneficial for applications such as biosensing[19-22], bioactive electro-responsive materials[23-25], tissue engineering scaffolds[26-29], and neuromorphic devices[30-33].

Mixed ionic/electronic conductors (MIECs)[34-35] have been applied to sensors[36-38], actuators[40], and organic electrochemical transistors (OECTs)[41-43]. In OECTs, an electrochemically driven ion insertion occurs in response to an electrochemical bias, which results in morphological reconfiguration and expansion to accommodate the volume of added ions.[44-45] OECTs have a significant advantage over organic field effect transistors (OFETs) in that ions injected into the material interact with the entire volume of the polymer and generate high transconductance signaling, desirable for biological sensing elements.[46-47] In general, a competitive OECT channel material requires the combination of good electronic transport, arising from high charge carrier mobility and effective ion penetration which increases the volumetric capacitance.[48] Understanding the properties of MIECs to control ion transport from electrolytes into the conjugated polymer is a fundamental consideration for various applications.

To enhance ion transport in CPs, functionalization with binding moieties can be useful. Systems such as poly(3-4-ethylenedioxythiophene) : poly(styrene-sulfonate) (PEDOT:PSS)[49-51], poly(3-hexylthiophene) (P3HT)[52-53], and poly(2-(3,3'-bis(2-(2-(2-methoxyethoxy)ethoxy)-ethoxy)-[2,2'-bithiophen]-5-yl)-thieno[3,2-b]thiophene (p(g2T-TT)[43,54], are very well known and well-studied for OECTs. The incorporation of glycolated analogs such as p(g2T-TT) has demonstrated the importance of side chain engineering, and resulted in the highest-performing OECT material reported.[55-57] P(g2T-TT) achieves high currents within sub-milliseconds time scale, high transconductance, and steep subthreshold switching.[58] Giovannitti et al[59] developed a donor-acceptor copolymer based on naphthalene-1,4,58-tetracarboxylic-diimide-bi-thiophene (NDI-T2) and progressively decreased the fraction of the alkyl side chain with a substituted glycol side chain. Copolymers with predominantly alkyl chains show high electron mobilities but those drop by orders of magnitude with the replacement by polar glycol chains.

Khau et al[60] demonstrated that a carboxylic acid functionalized polythiophene exhibits unipolar p-channel OECT operation in accumulation mode, competitive volumetric capacitance, and high transconductance, putting its performance among the highest among polymers with ionic side chain moieties. Conjugated polymers with modified hydrophilic side chains are being investigated for OECTs in both p-type and n-type organic semiconductors.[40] Hydrophilic side chains can enhance the ionic interaction and transport of bio-relevant ions such as Na^+, Cl^-, K^+, Ca^{2+}, PO_3^- and HCO_3^-.[61]

When a conjugated polymer is in contact with an electrolyte and a pair of metal electrodes, the conjugated polymer can accept electronic carriers, while counterions in the electrolyte solution can migrate into the polymer matrix to compensate for those carriers. This is formally known as

electrochemical oxidation and reduction but informally known as electrochemical doping.[48,62-63] The dependence of the electronic transport on the counterion is a relatively little studied area. Flagg et al[53] performed a comprehensive study of the role of dopant ions in mixed ionic/electronic conduction using P3HT-based OECTs as a model for investigating the role of the dopant ion. Doping PEDOT : PSS with an ionic liquid has also shown to dramatically increase OECT performance by improving the ion mobility that results from enhancing the ionic character of PEDOT : PSS.[64] Dong et al[65] performed a systematic study on morphological structure and ionic conduction between two polythiophene derivatives that incorporate glycol side chains adjacent to Li bis(trifluoromethanesulfonimide) (TFSI) as the electrolyte. Prefered electrolytes for OECTs induce high ionic conductivity, reducing the polarization time and increasing stability.[66]

In this work, polymers with the same thiophene backbone structure are used to make controlled comparisons among electrolyte ion properties and effects of polar side chain substituents. Five thiophene polymers that contain alkyl (-$(CH_2)_nCH_3$), ethyl ester (-COOR), poly(ethylene glycol) (-$O(CH_2CH_2O)_2CH_3$), hydroxyl (-OH), and carboxylic acid (-COOH) side chain functional groups are included. The OH polymer was newly synthesized. Additionally, potassium-based salts that vary in size, shape, and chemical composition of the anions, namely KCl, $KClO_4$, KPF_6, and KTFSI, were investigated. The ionic radius, anhydrous volume, and polarizability progressively increase while the hydration number in bulk water decreases. Homopolymers were first studied, and then combinations of polymers with pairs of the functional groups were blended. The essential findings are that the importance of the counterion dependence on OECT parameters varies greatly with the side chain functionality, and that some functional

group pairs lead to performance that can exceed that of the individual components. These findings are concentrated on pages 12-21.

2 Results

Polymer design and Synthesis

Polymers functionalized with an ethyl ester (PTCOOR) or carboxylic acid (PTCOOH) terminated side-chain were purchased from Rieke metals and had a reported average regioregularity of 84-85%. A very well-known alkylated side chain polymer poly(3-hexylthiophene), known as P3HT, a glycolated side chain polymer known as P3MEEMT, and a newly synthesized and previously unreported hydroxyl terminated side polymer that will be called PTOH were prepared. Figure 1 displays the chemical structure of the varied terminal side-chain functionalized polythiophenes being investigated. The three latter polymers were synthesized via Kumada catalyst-transfer polycondensation (KCTP)/ Grignard Metathesis (GRIM) polymerization, which is a versatile method for producing regioregular polythiophenes with good electronic transport properties.[67-69] The syntheses of the monomers and polymers are outlined in the Supporting Information, including ^{1}H NMR and GPC spectra shown in Figures S1-S8 and S9-S10, respectively. The synthesized polymers displayed good regioregularity (>90%). The polydispersity indices (PDIs), which influence the nanostructures formed by self-assembly, are

reasonable and generally narrow; however, the PDI from P3MEEMT is slightly wider but within commonly reported PDIs of polymers with oligoether side chains.[52,57,70]

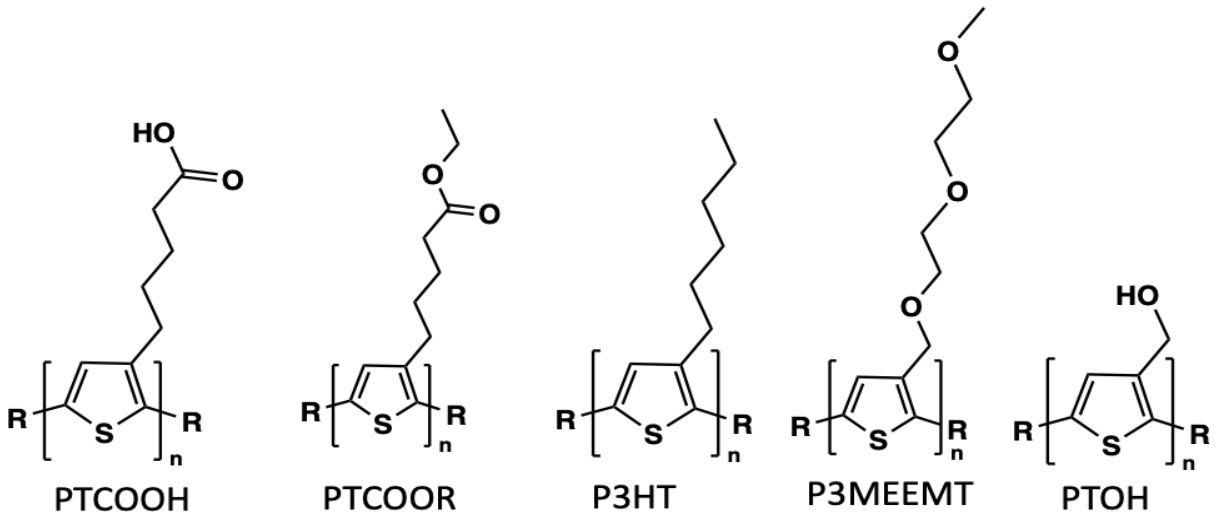

Figure 1. Chemical structure of varying terminal side-chain functionalized polythiophenes.

The UV-visible absorption spectra of the polymers as spun-coated thin films are shown in Supporting Information, Figure S11, and the data are summarized in Table 1.

Table 1. Thermal and Optical Summarization of functionalized homopolymers. [A] Melting temperature (T_m) and crystallization temperature (T_c) determined by DSC. [b] Optical band gap estimated from the low-energy band edge in the optical spectrum. PTOH and PTCOOH do not have measured enthalpy of fusion due to broadness of enthalpic peak indicating amorphous state.

Polymer	T_m^a (°C)	T_c^a (°C)	ΔH(T_c) (J/g)	Thin Film (nm)	E_g,opt[b] (eV)
P3HT	206	157	50.2	483, 530, 559, 611	1.70
PTCOOR	207	137, 181	29, 74	451, 484, 547, 608	1.70
P3MEEMT	106	151	-	482, 533, 618	1.60
PTOH	233	180	-	483, 536	1.70
PTCOOH	215	180	-	454, 483, 544, 595	1.60

The spectral shape and degree of structural order in the solid state of the polymer films are roughly similar, with the appearance of clearly defined vibronic shoulders to the right of the maximum absorption peak for systems defined by P3HT, PTCOOR, PTCOOH, and P3MEEMT, which indicates intermolecular interactions. P3HT displays the distinct π-π^* transition with λ_{max} at 550 nm (2.25 eV) and a shoulder starting at 608 nm (2.04 eV). P3HT displays appropriate agreement with what has been reported of λ_{max} at 2.23 eV and a shoulder at 2.06 eV.[71-72] It is reported that addition of polar side chains should cause a gradual blue-shift which can be related to J- and H- like aggregates.[73-74] PTCOOR has a λ_{max} at 532 nm (2.33 eV) and a shoulder starting at 610 nm (2.03 eV), PTCOOH has a λ_{max} at 531 nm (2.34 eV) and a shoulder starting at 599 nm (2.07 eV), PTOH has a λ_{max} at 529 nm (2.34 eV) with no visible shoulder, and P3MEEMT has a λ_{max} at 525 nm (2.36 eV) and a shoulder starting at 615 nm (2.02 eV). It should be noted that thinner films obtained from the more polar polymers made a negative artifact around 550 nm more pronounced, which could have altered some λ_{max} values. From the literature, poly(hexyl thiophene-3-carboxylate) was reported to have features at 395 nm (sh) and 475 nm while poly(octyl thiophene-3-carboxylate was reported with features at 410 nm (sh) and 469 nm.[75] Poly(octylthiophene-3-carboxylate) was additionally reported to have a λ_{max} at 444 nm while also exhibiting a large absorption at wavelengths lower than 350 nm, which indicates some oligomers being present.[76] Another report shows that the ester-functionalized P3AET (Poly(3-(2-aetoxyethyl)thiophene) has a λ_{max} at 440 nm in the film state and P3HET (Poly(3-(2-hydroxyethyl)thiophene) at 440 nm as well.[77] An additional study was conducted by Bilger et al[78] on the hydrogen-bonding induced ordered assembly of poly(3-alkylthiophene) derivatives bearing carboxylic acid groups (regioregularity 90-95% HT-HT) from diluted solution, concentrated

solutions, and solid films. Broad Gaussian-like absorption peaks are observed for P3C3T and P3C4T with λ_{max}'s of 442 and 464 nm, respectively. However, the absorption of P3C6T exhibited two peaks with narrow half-widths at 590 and 550 nm corresponding to $I^{0\text{-}0}{}_{abs}$ and $I^{0\text{-}1}{}_{abs}$ vibronic transitions, respectively. This is reported to correspond to the Frank-Condon progression of C=C stretching within the thiophene ring. Therefore, alkyl-chain length results in hypsochromic and bathochromic shifting of the spectra. The λ_{max} of P3MEEMT was reported to be 500 nm.[79] Deviations in optical properties can also occur due to the degree of planarity of the polymer backbone to which degrees in variation is caused by polymerization methods. For instance, head-to-head (H-H) linkages in the backbone of a polymer will result in interrupted conjugation due to the steric twist. Most of the reported literature polymers were synthesized via chemical oxidation, such as with $FeCl_3$, which resulted in a 55% HT-HT coupling structure for P3HET and P3HET. Poly(octylthiophene-3-carboxylate) was prepared via Ullmann reaction with a H-H/H-T ratio of 2.16: 1. Therefore our homopolymers display spectra consistent with the high regioregularity.

We also prepared 50/50 blend solutions and films as outlined in the Methods section. UV-visible absorption spectra of blend films are shown in the Supporting Information Figure S12 . If P3HT is blended with PTCOOR or P3MEEMT the λ_{max} shifts to 528 nm (2.35 eV) and 524 nm (2.37 eV), respectively. This is a hypsochromic shift (blue shift) by about 22-26 nm. Blending two polar side-chain polymers leads to much smaller shifts. It is expected that incorporating polar side chain results in an observable blue shift that should occur along with a significant decrease in $A^{0\text{-}0}/A^{0\text{-}1}$ because of the increase in disorder within the polymer aggregates. On the other hand, hydrogen bonding among side chains can cause a bathochromic effect.[80]

Thin Film Morphology

As shown in the Supporting Information, Figure S13, the XRD diffraction pattern was obtained for the homopolymers alone (Figure A), and the combinatorial blends in Figure B-F at room temperature for polymer films that were drop-cast on Si/SiO_2 (300 nm of thermal oxide) substrate. In Figure A, P3HT exhibits crystalline order with diffraction peaks at 2θ = 5.6° and 10.6°. These two peaks correspond to the (100) and (200) indices, respectively, of the unit cell for P3HT. The sharp intensity at the (100) index indicates high crystallinity. A study had been done that reported the differentiation of XRD patterns of P3HT. A slow-dried film should exhibit crystalline order with diffraction peaks at 2θ = 5.4°, 10.8°, 16.4°, and 23°, which corresponds to the (100), (200), (300), and (010) indices.[81] However, the lack of visibility of the higher order reflections may indicate that the film thickness is very low for suitable peak resolution. PTCOOR exhibits crystalline order with diffraction peaks at 2θ = 5.6°, 10°, and 15°, which corresponds to the (100), (200), and (300) indices. Another study using a very similar ester functionalized polythiophene polymer reported that distinct diffraction peaks at 2θ = 3.5° and 7.0° correspond to an inter-chain d-spacing of 24.7 Å and 12.6 Å, respectively.[82] However, for our ester functionalized polythiophene moiety, there is a concomitant disappearance of the π-π stacking occurring at 2θ = 23.2 (010) which means that our polythiophene functionalized with an ester displays highly ordered lamellar π-stacks.[83] PTCOOH displays broad features at 2θ = 6.3° and 13.8° with a broad peak beginning at 20°. A broad feature centered at 20° usually corresponds to disordered chains for P3HT, but for PTCOOH it is more indicative of the amorphous networks and has been similarly reported with a related polymer such as poly(thiophen-3-yl-acetic acid (PTAA) where no feature is formed for the polythiophene-based polymers.[84] Similar observations

are made on P3MEEMT and PTOH. No observable feature or intensified sharp peaks were detected, which could limit the ability of our XRD study to designate a fully amorphous state or find crystalline domains within these materials. In addition, it was reported that a broad peak for a functionalized ester polythiophene was observed at 2θ = 24.7°. which indicates π-π stacking distance observed in other thiophene polymers (3.5-3.8 Å).[82,85] Therefore, depending on the functional group on the side-chain of the polythiophene, the broad features appears stronger, which can be seen in PTCOOH, PTOH, and P3MEEMT, which may indicate disorder.

The blended films in Supporting Information, Figure S13 B-F showed a merging of the individual polymers. Figure B. P3HT blended with P3MEEMT displayed the usual crystalline feature of 2θ = 5.6° for the (100) index; however, the (200) index is lost and is replaced by the amorphous disordered region occurring at higher 2θ. P3HT blended with PTCOOR preserves the indices found in pure PTCOOR where the distinct (100), (200), and (300) indices of the unit cell are still observed but the higher index (300) seems less pronounced with (200) index becoming less distinct and broader. PTCOOR blended with P3MEEMT results in the complete loss of (200) index and more pronounced 2θ=5.6° and 16.3°. Blending PTCOOR and PTOH results in more defined amorphous broad regions; however, the distinct (100) index occurring at 2θ=5.6 becomes significantly lower and less intense and sharpness is reduced. This indicates that there is less crystallinity, crystals are smaller, and/or more defective.[81] PTCOOR blended with PTCOOH results in more pronounced and intense peaks than are observed from PTCOOH alone. As a matter of fact, all polymers (P3MEEMT, PTOH, and PTCOOR) blended with PTCOOH show an increase in the intensity of the (100) reflection as well as the observable (300) reflection. It is possible that

the different functionalities of these polymers led to more structural order, larger crystal sizes, and/or fewer defects. PTOH retains amorphous characteristics except with PTCOOH.

Polymer Thermal Properties

Differential scanning calorimetry (DSC) was performed to determine the thermal transitions of each polymer. The polymers were heated at a ramp rate of 10°C/min and then cooled at a ramp rate of 20°C/min under a nitrogen atmosphere. The detailed thermal traces are found in the Supporting Information, Figure S14, and a corresponding compilation of properties is presented in Table 1. P3HT exhibits one endothermic peak at 206°C and one single exothermic peak upon cooling at 157°C. This is very similar to already published values of P3HT where it is reported that P3HT displays an endothermic peak at around 233°C and a reported exothermic peak at 194°C.[85] The enthalpy of calculated fusion (ΔH_m) was 50.2 J/g which is equivalent to reports of 42.2 J/g for extended chain crystals of oligomeric P3HT to infinite molecular weight.[86] For PTCOOR, it is interesting to note the double exotherms upon cooling, which may indicate the presence of different polymorphs, a second phase, or even structure change. However, there are two exotherms at 137°C and 181°C, and a single endothermic peak at 207°C. A report on an ester functionalized polythiophene that crystallizes at 177 °C and has a sharp endothermic transition upon heating at 180°C is similar to the PTCOOR polymer that is being studied.[82] The enthalpy of fusion ((ΔH_m) was calculated as 29 J/g and 74 J/g. P3MEEMT was much more fragile in the sense that the maximum applied temperatures had to be lower, but it displayed one broad exothermic peak at 151°C and one endothermic peak at 105°C. A study had been conducted on P3MEEMT where three crystallite melting temperatures at about 60°C, 125°C (strong peak), and 150°C were found, suggesting polymorphs. In addition, the crystallite reformation occurred at roughly 125°C

and 65°C.[87] The PTOH and PTCOOH had very similar thermograms in that there is a single exothermic peak both situated at 180°C, while the endothermic peak was very broad and resided at 220°C and 215°C, respectively. In a published study, the presence of broad peaks, indicating glass transitions, further confirms the amorphous nature of PTOH, PTCOOR, PTCOOH, and P3MEEMT as well as the presence of intermolecular hydrogen bonding.[88]

Electrical Characteristics

A thin film of each polymer was spin-coated onto each individual OECT substrate purchased from NanoSPR. The film thickness was measured by profilometer and ranged from 200-300 ± 50 nm. The transistor channel length is 10 μm and the total width is 20 mm (20 interdigitated pairs of 1 mm each). The W/L ratio is reported and validated by NanoSPR as being 2000. Four electrolytes were studied with each polymer. The electrolytes consisted of KCl (1M), $KClO_4$ (1 M), KPF_6 (1M), and KTFSI (1M). The gate electrode is an Ag/AgCl (3.5 M) reference electrode immersed in KCl solution. Further details of OECT, film fabrication, and electrolyte preparation are provided in the Methods section.

The generated transfer characteristics are shown in Figure 2, and Table 2 displays a compilation of properties of the homopolymers. The 5 polymers are p-type and by applying a negative gate voltage (V_g), the anions will diffuse and be injected into the polymer. This will generate an increase in the hole concentrations resulting in higher drain current (I_D).

Table 2. Electrical Properties and Characteristics. Compiled tables of transfer characteristic performance of each anion varying electrolyte subjected to A) P3HT, B) PTCOOR, C) P3MEEMT, D) PTOH, and E) PTCOOH. Each representative table consists of the V_{TH} in the forward 0 to -1 V direction, V_{TH} in the -1 to 0 V reverse direction, potential of $G_{m,max}$ in forward and reverse direction. Transconductance (G_m) max in the forward and reverse direction. Key data are indicated in red boxes.

A

P3HT	V_{TH} (F) (mV)	V_{TH} (R) (mV)	$G_{m,P}$ (F) (mV)	$G_{m,P}$ (R) (mV)	G_m (F) (mS)	G_m (R) (mS)
KCl	-910±30	-500±40	-1000	-750±50	0.48±1	0.4 ± 0.3
$KClO_4$	-740±20	-440±70	-960±30	-800±50	64±10	30±5
KPF_6	-690±30	-360±40	-970±20	-870±30	70±10	60±10
KTFSI	-500±20	-400±20	-860±20	-850±30	76±20	74±20

B

PTCOOR	V_{TH} (F) (mV)	V_{TH} (R) (mV)	$G_{m,P}$ (F) (mV)	$G_{m,P}$ (R) (mV)	G_m (F) (mS)	G_m (R) (mS)
KCl	-780±30	-770±10	-990±10	-930±20	33±5	31±5
$KClO_4$	-550±30	-270±80	-820±10	-750±30	54±5	51±5
KPF_6	-450±30	-260±60	-800±10	-780±50	54±10	58±10
KTFSI	-240±10	-200±20	-700±50	-670±30	60±10	70±10

C

P3MEEMT	V_{TH} (F) (mV)	V_{TH} (R) (mV)	$G_{m,P}$ (F) (mV)	$G_{m,P}$ (R) (mV)	G_m (F) (mS)	G_m (R) (mS)
KCl	-780±20	-800±30	-930±20	-990±0	3.3±1	6.4±2
$KClO_4$	-630±10	-600±20	-990±10	-930±10	35±10	36±10
KPF6	-580±10	-560±10	-970±30	-940±10	44±5	44±10
KTFSI	-700±200	-600±400	-900±60	-1000±10	0.39±0.1	0.49±0.1

D

PTOH	V_{TH} (F) (mV)	V_{TH} (R) (mV)	$G_{m,P}$ (F) (mV)	$G_{m,P}$ (R) (mV)	G_m (F) (mS)	G_m (R) (mS)
KCl	-540±20	-470±40	-890±20	-860±20	35±10	30±10
$KClO_4$	-570±20	-460±10	-920±30	-850±10	38±1	35±2
KPF_6	-560±20	-480±20	-960±30	-890±10	35±5	28±5
KTFSI	-400±5	-310±10	-820±10	-740±20	48±10	46±10

E

PTCOOH	V_{TH} (F) (mV)	V_{TH} (R) (mV)	$G_{m,P}$ (F) (mV)	$G_{m,P}$ (R) (mV)	G_m (F) (mS)	G_m (R) (mS)
KCl	-240±50	-230±40	-810±40	-830±50	50±10	50±10
$KClO_4$	-200±30	-180±30	-740±40	-790±30	55±10	50±10
KPF6	-210±20	-180±40	-790±40	-820±50	48±10	50±10
KTFSI	-230±20	-200±20	-730±40	-710±50	50±10	60±20

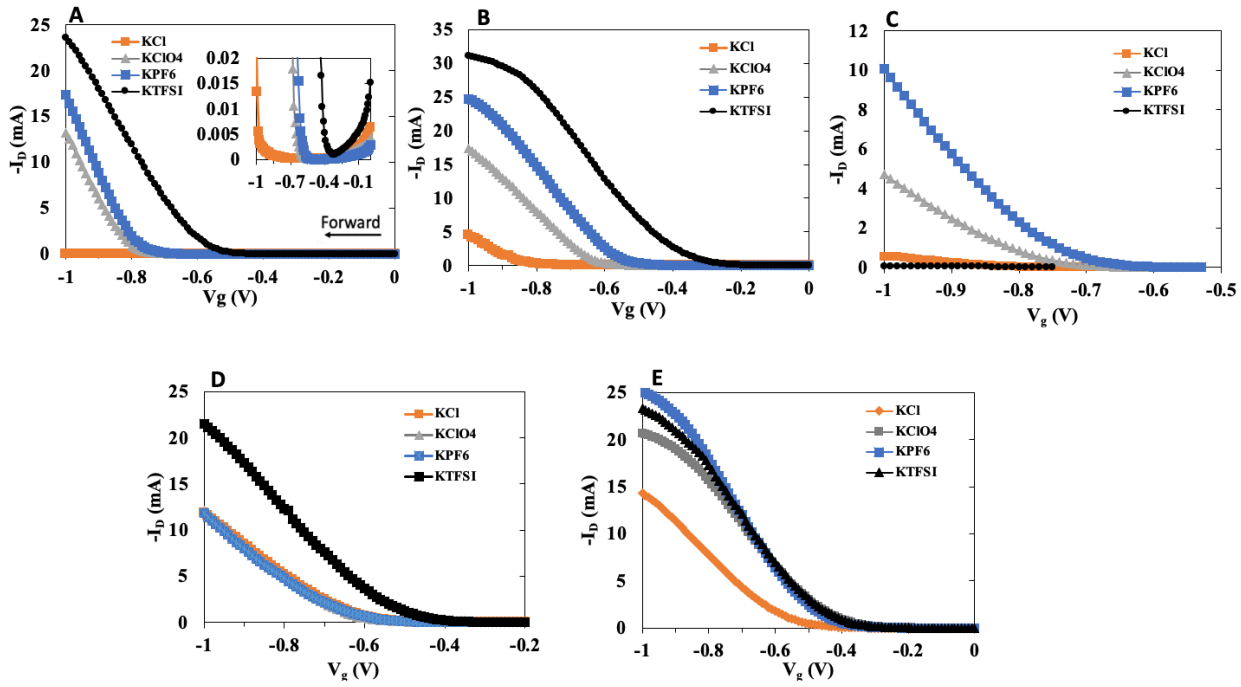

Figure 2. Transfer curves of functionalized polythiophene motifs configured as electrochemical transistors. Characteristic transfer curves (V_D = -600 mV) are displayed for A) P3HT, B) PTCOOR, C) P3MEEMT, D) PTOH, and E) PTCOOH tested with 4 varying anions of the potassium salts [chloride, perchlorate, hexafluorophosphate, and bis(trifluoromethanesulfonyl)imide] at an electrolyte concentration of 1 M. Vg is properly denoted as V vs Ag/AgCl with correspondence to the reference electrode.

It was already reported by Flagg et al[53] that the output currents, threshold voltages (V_{TH}), and injected charge densities in P3HT OECTs depend strongly on the anion electrolyte. In general, with larger molecular anions, V_{TH} was lowered, and greater transistor currents are generated. This same trend is seen strongly in Figures 2A, 2B, and 2C, but only slightly for the more polar polymers of Figures 2D and 2E. P3HT had an initial V_{TH} of -910 ± 30 mV with KCl but that shifted to -500 ± 20 mV when a much larger TFSI anion was used. PTCOOR displayed a similar trend; however, the shift was more prominent with each anion. PTCOOR had an initial V_{TH} of -

780 ± 30 mV with KCl but that reached -240 ± 10 mV with TFSI, a 69% decrease. P3MEEMT on the other hand displayed a large magnitude V_{TH} shift up to KPF_6; but, when a high concentration of KTFSI was applied to P3MEEMT a very strong decrease in I_D is observed and immediate shift of V_{TH} to more negative potentials is observed. This can possibly be explained by the electrolyte driving a large change in the polymer microstructure. It was reported by Matta et al[89], through XRF and MD simulations, that different counterions had varied effects on the p(g2T-TT)-water interface and that softer polyatomic anions such as $TFSI^-$ and ClO_4^- can enhance metal coordination and result in chelation by the ethylene glycol side chains. In addition, the hydrophobic character of $TFSI^-$ can result in the higher tendency of the anion to concentrate at the interface of the polymer electrolyte environment and result in higher cation-side chain chelation. It was also reported that the polymer side chains can be completely saturated by the cation coordination sphere if $TFSI^-$ is used as the counterion. K^+ has a higher propensity to swap loosely bound water solvation for the glycol side chains of P3MEEMT. Therefore, with the chelating capabilities of K^+ cation being strong, it prevents the $TFSI^-$ anion from being injected into the polymer resulting in insufficient doping, which is observed in the significant decrease in I_D but also return of the V_{TH} to the same value as for KCl. PTOH, on the other hand, displayed a unique consistency using KCl, $KClO_4$, and KPF_6. It was not until a larger anion such as KTFSI was used that a noticeable shift in the V_{th} occurred (shift of 26%) as well as an increase in the I_D. PTCOOH had a varying response in the sense that all anions larger than Cl^- shifted the threshold voltage by roughly the same small magnitude (about 17% decrease).

Supporting Information, Figure S15, displays all the output curves generated of the functionalized homopolymers that are individually tested with each anion electrolyte. The

polymers all display OECT device behavior, and the magnitude of I_D increases as the anion electrolyte changes with the increase in anion size, volume, and polarizability.[53] As the anions are injected into the semiconductor film, volumetric doping occurs resulting in the increase in I_D which is consistent with accumulation mode operation. P3HT originally displays a response when V_g is held at or above -700 mV for KCl, $KClO_4$, and KPF_6 anions. In the ideal case of a transistor output curve, I_D linearly increases at low V_D and becomes saturated at a constant level. However, in realistic devices, output curves are not perfectly flat at high V_D which is due to channel length modulation, space-charge-limited conduction through depleted semiconductor, and electric field dependence of mobility.[90] This can be seen with P3HT with $KClO_4$ and KPF_6 electrolyte. However, the working operation is greatly enhanced with KTFSI as the electrolyte. PTCOOR and PTOH both display more ideal transient OECT device charateristics compared to P3HT and enhanced I_D generation. P3MEEMT initially does not display any response until a much larger Vg is applied with KCl; however, more ideal transient behavior is obtained with $KClO_4$ and KPF_6. As earlier described, KTFSI results in de-doping and a loss of strength in transient behavior.

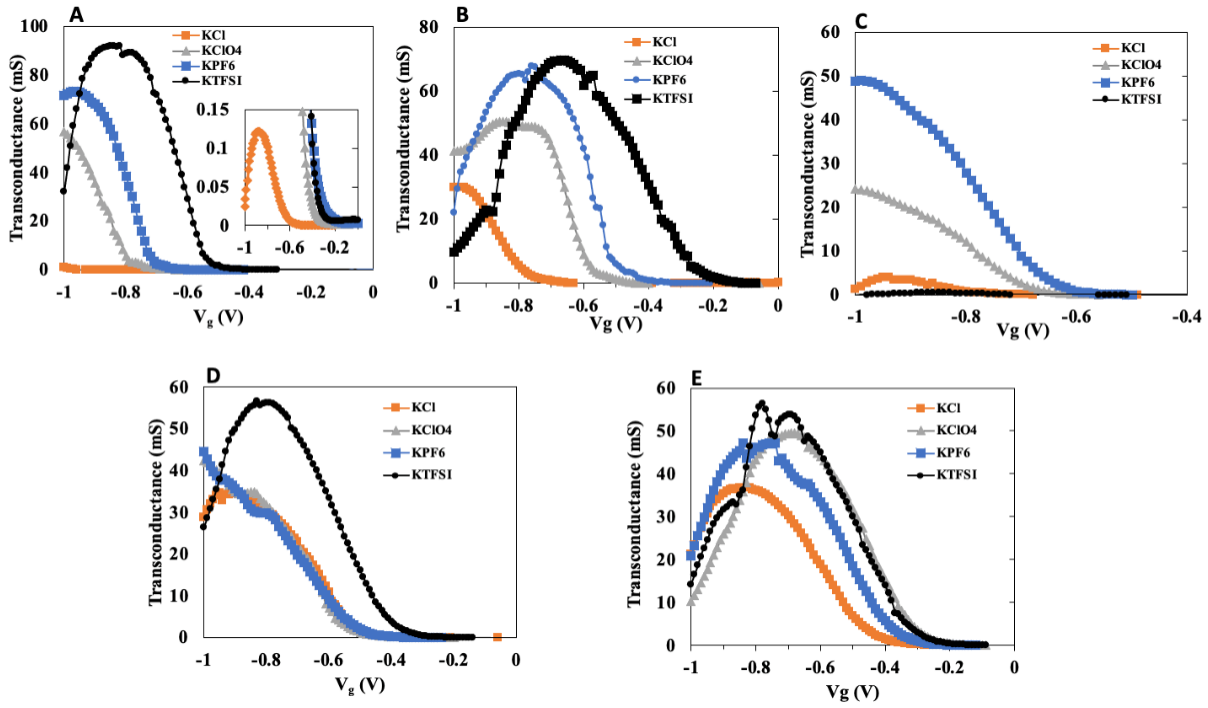

Figure 3. Transconductance of functionalized polythiophene motifs. Characteristic transconductance values (V_D = -600 mV) are displayed for A) P3HT, B) PTCOOR, C) P3MEEMT, D) PTOH, and E) PTCOOH tested with 4 varying anions of the potassium salts [chloride, perchlorate, hexafluorophosphate, and bis(trifluoromethanesulfonyl)imide] at an electrolyte concentration of 1 M. Vg is properly denoted as V vs Ag/AgCl with correspondence to the reference electrode.

Figure 3 displays the transconductance plots, and Table 2 displays the compiled values. The non-OH polymers P3HT, PTCOOR, and P3MEEMT had significantly higher transconductance. P3HT initially had a transconductance value of 0.5 ± 1 mS with Cl^- but this was greatly enhanced to 64 ± 10 mS, 70 ± 10, and 76 ± mS when using ClO_4^-, PF_6^-, and $TFSI^-$, respectively. Flagg et al[53], had initially stated that P3HT does not demonstrate high transconductance but emphasizes the importance of favorably tailoring the ion-polymer interaction to improve its properties. The same demonstration can be seen with PTCOOR and P3MEEMT where the transconductance value

increases, but the magnitude of increase is dependent on the anion size and functional moiety that is present. It was reported by Flagg et al[52], that P3MEEMT transconductance increases from about 1000 μS to 4000 μS from switching from 100 mM of KCl to 100 mM of KPF_6 with a device configuration of W/L ratio of 10 and 80 nm thickness films. The geometric parameters of the OECT channel also define transconductance, so comparisons can only be made within single systems within our experiment. PTOH and PTCOOH show relatively stable transconduction for different anions. However, it is noticeable that the potential peak transconductance value shifts to lower V_g. PTCOOR displays the largest shift in transconductance potential where the peak initially is found at -1 V but shifts to -0.65 V. The curve shapes are different for the various anions, which could affect their applicable voltage ranges.

Figure 4 and Table 3, display the transfer curves and summarize transfer characteristics of the 50/50 mixed blends of the polymers. Note that it was not possible to make compatible mixtures of P3HT with PTOH or PTCOOH.

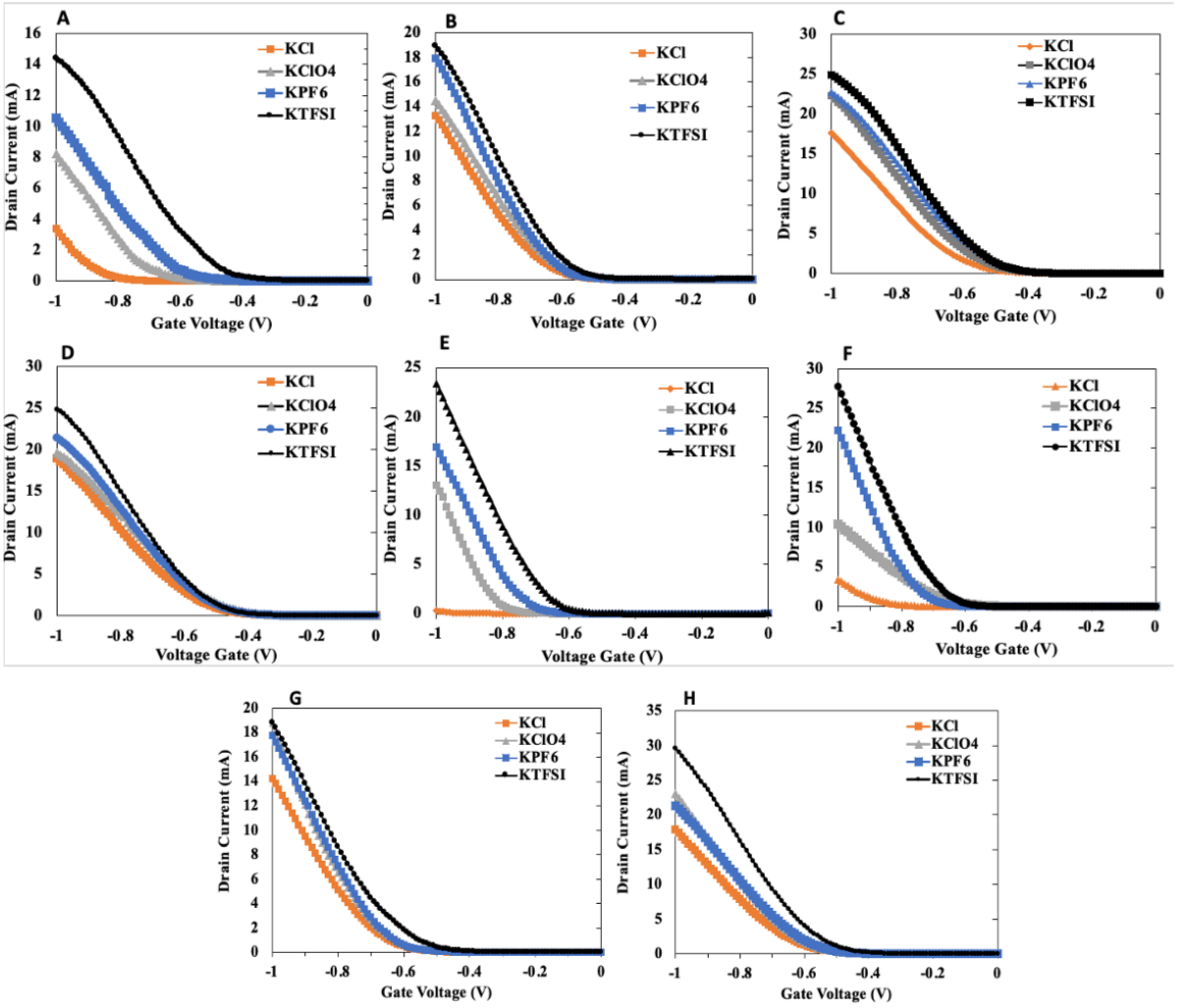

Figure 4. Transfer curves of functionalized polythiophene motifs as 50/50 mixed blends configured as electrochemical transistors. Characteristic transfer curves (V_D = -600 mV) are displayed for A) P3HT/PTCOOR, B) PTCOOR/PTOH, C) PTCOOR/PTCOOH, D) PTOH/PTCOOR, E) P3MEEMT/P3HT, F) P3MEEMT/PTCOOR, G) P3MEEMT/PTOH, and H) P3MEEMT/PTCOOH tested with 4 varying anions of the potassium salts [chloride, perchlorate, hexafluorophosphate, and bis(trifluoromethanesulfonyl)imide] at an electrolyte concentration of 1 M. V_g is properly denoted as V vs Ag/AgCl with correspondence to the reference electrode.

Table 3. Compiled tables of transfer characteristic performance of each anion varying electrolyte subjected to combinatorial 50:50 mixed blends of A) P3HT/PTCOOR, B) PTOH/PTCOOR, C) PTCOOH/PTCOOR, D) PTCOOH/PTOH, E) PTCOOH/PTOH, F) P3MEEEMT/PTCOOR, G) P3MEEMT/PTOH, H) P3MEEMT/PTCOOH . Each representative table consists of the V_{TH} in the forward 0 to -1 V direction, V_{TH} in the -1 to 0 V reverse direction, potential of $G_{m,max}$ in forward and reverse direction. Transconductance (G_m) max in the forward and reverse direction. Key data are indicated in red boxes.

A

P3HT/ PTCOOR	V_{TH} (F) (mV)	V_{TH} (R) (mV)	$G_{m,p}$ (F) (mV)	$G_{m,p}$ (R) (mV)	G_m (F) (mS)	G_m (R) (mS)
KCl	-780±20	-670±50	-990±30	-960±20	30±5	17±3
$KClO_4$	-560±10	-400±60	-910±30	-870±20	80±20	60±10
KPF_6	-470±30	-340±40	-870±30	-810±40	70±5	56 ± 5
KTFSI	-320±40	-230±30	-750±30	-700±60	70±3	65±10

B

PTOH/ PTCOOR	V_{TH} (F) (mV)	V_{TH} (R) (mV)	$G_{m,p}$ (F) (mV)	$G_{m,p}$ (R) (mV)	G_m (F) (mS)	G_m (R) (mS)
KCl	-520±10	-440±10	-930±30	-870±10	52±10	45±10
$KClO_4$	-500±10	-410±10	-900±30	-830±20	43±10	39±5
KPF_6	-540±10	-420±20	-890±10	-850±20	48±5	42±5
KTFSI	-480±20	-320±5	-820±20	-750±10	52±5	44±5

C

PTCOOH/ PTCOOR	V_{TH} (F) (mV)	V_{TH} (R) (mV)	$G_{m,p}$ (F) (mV)	$G_{m,p}$ (R) (mV)	G_m (F) (mS)	G_m (R) (mS)
KCl	-400±10	-360±20	-830±30	-810±30	54±10	54±10
$KClO_4$	-360±10	-310±40	-760±30	-750±30	60±5	60±5
KPF_6	-360±20	-340±30	-800±10	-780±30	69±20	69±20
KTFSI	-380±10	-350±10	-820±10	-780±20	68±5	68±10

D

PTCOOH/ PTOH	V_{TH} (F) (mV)	V_{TH} (R) (mV)	$G_{m,p}$ (F) (mV)	$G_{m,p}$ (R) (mV)	G_m (F) (mS)	G_m (R) (mS)
KCl	-310±50	-280±40	-845±30	-900±30	47±10	54±4
$KClO_4$	-270±20	-215±20	-840±20	-870±50	49±10	50±6
KPF_6	-190±40	-170±40	-750±10	-740±50	53±10	56±10
KTFSI	-280±20	-230±20	-800±30	-770±30	58±10	56±10

E

P3MEEMT/ P3HT	V_{TH} (F) (mV)	V_{TH} (R) (mV)	$G_{m,p}$ (F) (mV)	$G_{m,p}$ (R) (mV)	G_m (F) (mS)	G_m (R) (mS)
KCl	-850±10	-670±60	-980±40	-800±20	3.5±2	1.8±1
$KClO_4$	-660±5	-580±20	-940±10	-880±20	70±10	60±10
KPF_6	-560±10	-470±30	-910±50	-870±10	80±20	60±10
KTFSI	-470±10	-370±20	-870±20	-820±20	75±10	70±10

F

P3MEEMT/ PTCOOR	V_{TH} (F) (mV)	V_{TH} (R) (mV)	$G_{m,p}$ (F) (mV)	$G_{m,p}$ (R) (mV)	G_m (F) (mS)	G_m (R) (mS)
KCl	-780±20	-990±20	-910±70	-960±20	30±4	20±4
$KClO_4$	-480±30	-410±40	-890±10	-850±20	70±20	60±10
KPF_6	-430±30	-370±40	-910±50	-870±10	90±10	80±10
KTFSI	-340±30	-320±30	-810±20	-790±20	80±20	75±20

G

P3MEEMT/ PTOH	V_{TH} (F) (mV)	V_{TH} (R) (mV)	$G_{m,p}$ (F) (mV)	$G_{m,p}$ (R) (mV)	G_m (F) (mS)	G_m (R) (mS)
KCl	-550±10	-450±10	-920±10	-880±40	50±10	40±3
$KClO_4$	-530±10	-440±20	-930±30	-840±40	60±20	50±10
KPF_6	-570±20	-470±40	-880±40	-860±30	40±10	30±10
KTFSI	-470±10	-380±20	-860±20	-770±10	50±10	40±10

H

P3MEEMT/ PTCOOH	V_{TH} (F) (mV)	V_{TH} (R) (mV)	$G_{m,p}$ (F) (mV)	$G_{m,p}$ (R) (mV)	G_m (F) (mS)	G_m (R) (mS)
KCl	-510±40	-480±10	-900±20	-880±40	40±10	50±10
$KClO_4$	-480±40	-460±30	-860±20	-850±30	50±10	50±20
KPF_6	-480±10	-450±20	-860±30	-830±10	50±10	50 ± 10
KTFSI	-410±10	-400±10	-830±30	-810±40	50±20	50±20

Mixed blends display a V_{TH} that is between those for the individual constituent polymers. For example, PTCOOH has an initial V_{TH} of -240 ± 50 mV and PTOH has an initial V_{TH} of about -540 ± 20 mV using 1.0 M of KCl. However, for a mixed 50/50 blend of PTCOOH/PTOH, V_{TH} is -310

± 50 mV. For mixed blends that are opposite in polarity or unfavorable in blending compatibility, for example PTOH/PTCOOR, the V_{TH} is dominated by the stronger ion-interacting species, which is PTOH in this case, but for PTCOOH/PTCOOR the initial V_{TH} is an intermediate value of -400 ± 10 mV. Therefore, depending on the functionality and favorability in blend synergist interaction, the V_{TH} can be adjusted as well.

Supporting Information Figure S16 displays all the output curves generated for the blended functionalized homopolymers. Most of the polymer mixtures generate ideal OECT transient behavior. Initially using KCl as the electrolyte, P3HT:PTCOOR blend displays a response when V_g is held at -700 mV; however, greater transistor response is observed at lower Vg application with larger anion electrolytes. Importantly, the very low currents observed with KCl and P3HT are increased when P3HT is blended with any of the other, more polar polymers. Also, the PTCOOH/PTOH and P3MEEEMT/PTCOOR blends showed some higher currents than did either of the individual polymers, evidence of some functional group synergy that could be explored in future studies.

Figure 5 displays the transconductance-V_g plots and Table 3 displays the compiled values. Again, functional group polarity seems to dictate the maximum transconductance value obtained. P3HT and PTCOOR, blends, having the least relative polarity, have the highest ultimate transconductance and potential window dependence on anion size. The more polar polymers have higher transconductance with KCl electrolyte. Blends of the

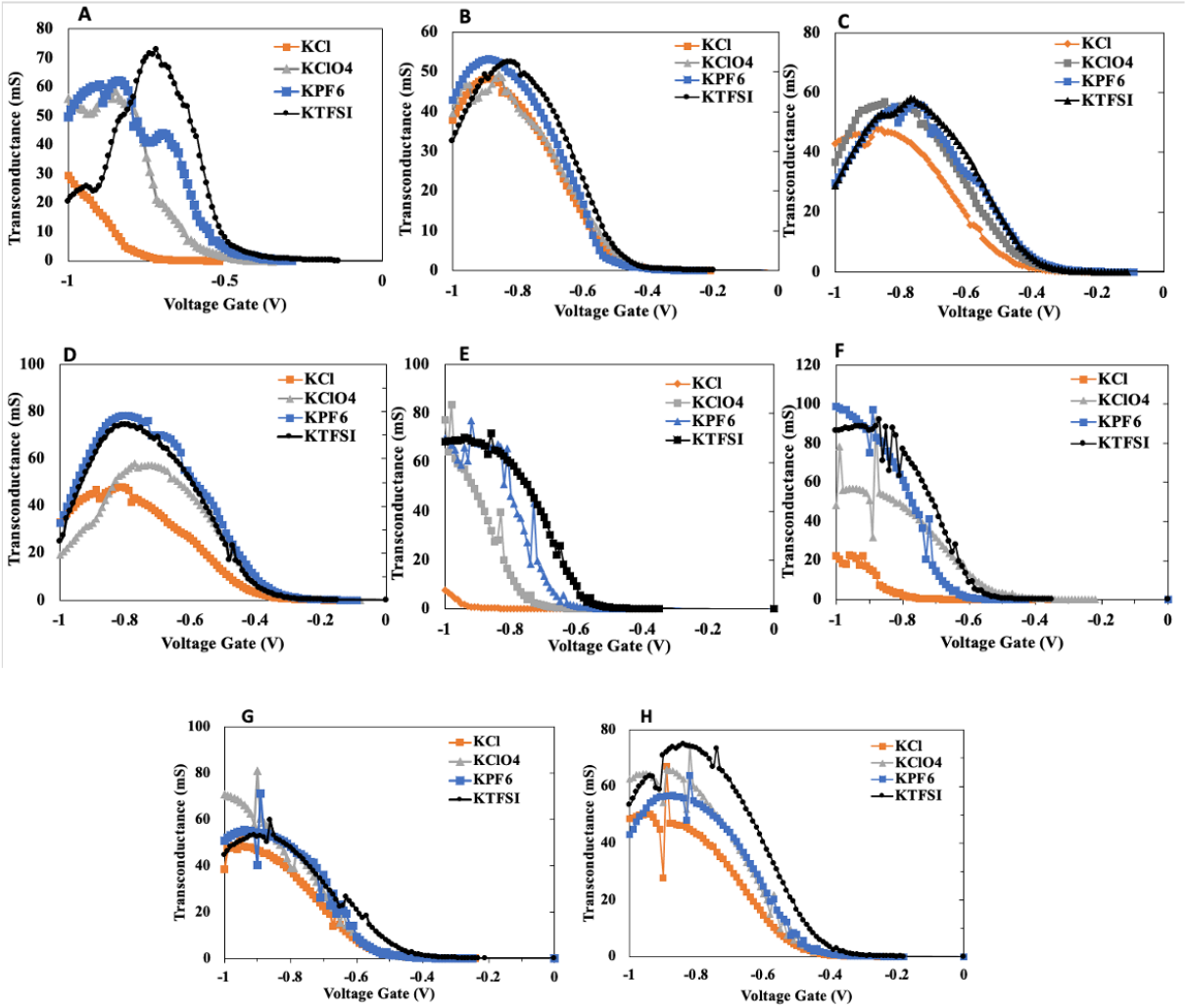

Figure 5. Transconductance of functionalized polythiophene motifs. Characteristic transconductance values (V_D = -600 mV) are displayed for A) P3HT/PTCOOR, B) PTCOOR/PTOH, C) PTCOOR/PTCOOH, D) PTOH/PTCOOR, E) P3MEEMT/P3HT, F) P3MEEMT/PTCOOR, G) P3MEEMT/PTOH, and H) P3MEEMT/PTCOOH tested with 4 varying anions of the potassium salts [chloride, perchlorate, hexafluorophosphate, and bis(trifluoromethanesulfonyl)imide] at an electrolyte concentration of 1 M. Vg is properly denoted as V vs Ag/AgCl with correspondence to the reference electrode.

non-OH polymers have the highest transconductances in the study, illustrating possible synergy between the organizational and ion-binding properties of the functional groups. However, polymers with high polarity seem to be less influenced by anionic species due to possible coordination of the cations, which does not have a large effect on V_{TH} or transconductance

increase. It is noted that even with the greater stability that polymers such as PTOH and PTCOOH have, very large anions such as $TFSI^-$ still can disrupt any coordination interaction resulting in a shift of V_{TH} and potential peak of the transconductance but only by a small magnitude.

Additional side chain-dependent electronic parameters

Figure 6 shows the cyclic voltammograms (CVs) of P3HT, PTCOOR, PTOH, and PTCOOH using 0.1 M $TBAPF_6$ in acetonitrile (MeCN) at a scan rate of 50 mV/s. Unfortunately, P3MEEMT is soluble in acetonitrile and could not be analyzed in this approach so it was omitted in this study. P3HT displays a reversible oxidation wave with small shoulder at the foot of the wave. The CVs are very similar to a published curves for P3HT with a M_W = 60 kDa using 0.1 M $TBAPF_6$.[91] Harris et al[92] noted the presence of two reversible oxidation waves for P3HT in 0.1 M TBAHFP as the supporting electrolyte. They indicate that the peak near 0.2 vs. $Ag/AgNO_3$ represents the oxidized aggregated domains of a larger conjugated length, but the peak near 0.6 V represents amorphous regions with short conjugation length that are less oxidizable.

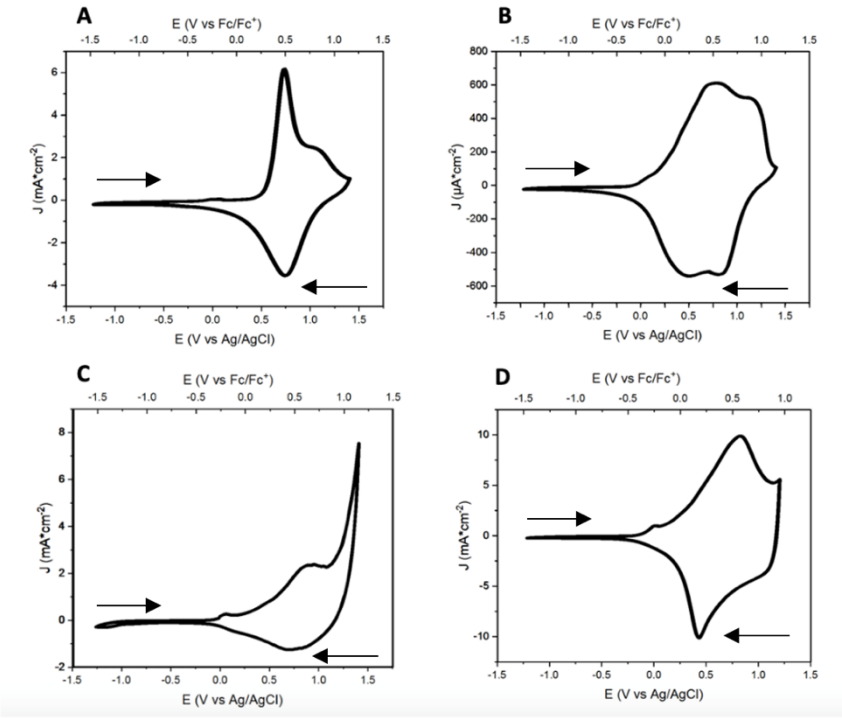

Figure 6. Thin film cyclic voltammograms of drop-cast polymers. A) P3HT, B) PTCOOR, C) PTOH, and D) PTCOOH on Pt electrodes in 0.1 M $TBAPF_6$ in MeCN at 50 mV/s. Arrows display scan direction.

We observe a reversible oxidation peak at 0.7 V vs Ag/AgCl which is reasonable since the M_w of our P3HT is roughly 16,000 while theirs is 47,000 and therefore might contain some shorter oligomers. Also, polythiophenes with moderate to high regioregularity are formally amorphous with a quasi-ordered phase dispersed in continuous disordered domains.[93] PTCOOR on the other hand displays two reversible oxidation waves with oxidation peaks located at 0.9 and 1.2 V vs Ag/AgCl, respectively. PTCOOH displays one reversible oxidation wave with an oxidation peak located at about 0.9 V vs Ag/AgCl as well. PTOH is observed to have a reversible oxidation peak (0.5 V vs Ag/AgCl) as well as well as a small broad shoulder at the foot of the wave (~ 1 V vs Ag/AgCl). Plots using other scan rates from 10 mV/s to 250 mV/s are also found in Supporting Information Figure S18-21.

Analysis was continued by calculating the band gaps and LUMO levels. P3HT has been reported to have a broad range of bandgap values derived from cyclic voltammetry, but the lowest unoccupied molecular orbital (LUMO) position was reported to range from -3.53 to -2.70 eV; while the highest occupied molecular orbital (HOMO) position is reported to range from -4.92 to -5.20 eV.[94-95] Table 4 compiles the results obtained by both UV-vis absorption and CV spectra analysis. P3HT was

Table 4. Electrochemical Property of Polymers from CV. Experimental HOMO energy levels were calculated from onset of oxidation peaks in CV. LUMO energy levels obtained from HOMO(onset of CV) and optical band gap using LUMO = HOMO + $E_{g,opt}$ (eV). Optical band gap calculated from onset of absorption spectra of polymers and listed in Table 1.

Polymer	$^aE_{onset}$ (V)	$^aE_{1/2}$ (V)	E_{HOMO} (eV)	E_{LUMO} (eV)
P3HT	0.292	0.56	-5.1	-3.4
PTCOOR	-0.212	0.40	-4.6	-2.9
PTOH	-0.02	0.60	-4.8	-3.1
PTCOOH	-0.30 V	0.67	-4.5	-2.9

measured to have a HOMO level of -5.1 eV and LUMO of -3.4 eV, which fits well with previous reports. Other polymers were similar in this regard. The energy levels were somewhat closer to vacuum with polar functionalities incorporated .

The parameters volumetric capacitance (C*) and mobility (μ) were determined to allow comparison with established benchmark polymers. To calculate C*, the specific capacitance (per unit mass) was calculated from the cyclic voltammetry (CV) curves obtained in 0.1 M KCl in H_2O (Supporting information Figure S22) according to the following equation defined below (the full derivation can be found in the methods section in the Supplementary Information.):[96-98]

$$C_p = \frac{A}{m*\left(\frac{V}{t}\right)*\Delta V};$$

By replacing m by the area of the electrode and then dividing the entire expression by the thickness of the film drop-cast onto the electrode generates the volumetric capacitance. Romele et al[99], had experimentally found that C* is independent of the ion concentration for PEDOT-PSS. The polymers in this study were calculated to have a C* value of 6 ± 5 F•cm^{-3}, 70 ± 40 F•cm^{-3}, 170 ± 20 F•cm-3, 140 ± 10 F•cm^{-3}, 160 ± 30 F•cm^{-3} for P3HT, PTCOOR, P3MEEMT, PTOH, and PTCOOH, respectively. Both P3HT and PTCOOH have already been reported to have a measured C* value of 40 F•cm^{-3} in 0.1 M $TBAPF_6$/DCM with 0.1 M NaCl using a liquid-liquid phase separation architecture[100]and 150 ± 18 F•cm^{-3} in 0.1 M NaCl/H_2O,[60] respectively. P3MEEMT was reported to have a C* of 294 F•cm^{-3} in KPF_6 electrolyte and 175 F•cm^{-3} in KCl electrolyte.[52] Therefore, volumetric capacitance of the polymers of this study are in good agreement with previously reported volumetric capacitance values.

The electronic carrier mobility μ associated with a swollen wet state, can be extracted by measuring the transconductance found in the OECT measurements using the equation:[52]

$G_m = \frac{W \bullet d}{L} \bullet \mu C^* \bullet (V_{th} - V_g)$;

where G_m is the transconductance, d is the film thickness, V_{th} is the voltage threshold, V_g is the gate bias, and W/L is the width over length ratio of the channel. The values we obtained were 2.7 x 10^{-2} ± 2.2 x 10^{-2} $cm^2 \bullet V^{-1} \bullet s^{-1}$, 4.5 x 10^{-2} ± 7.2 x 10^{-3} $cm^2 \bullet V^{-1} \bullet s^{-1}$, 6.4 x 10^{-3} ± 1.1 x 10^{-3} $cm^2 \bullet V^{-1} \bullet s^{-1}$, 1.4 x 10^{-2} ± 4.0 x 10^{-3} $cm^2 \bullet V^{-1} \bullet s^{-1}$, and 1.0 x 10^{-2} ± 3.1 x 10^{-2} $cm^2 \bullet V^{-1} \bullet s^{-1}$ for P3HT, PTCOOR, P3MEEMT, PTOH, and PTCOOH, respectively. Comparing these values to already published values, Flagg et al[53] reported P3HT μ to converge and saturate near 10^{-2} $cm^2 \bullet V^{-1} \bullet s^{-1}$ and attributed this to unannealed films and variation of regioregularity. As an OFET, P3MEEMT exhibits a mobility of 3 x 10^{-4} $cm^2 \bullet V^{-1} \bullet s^{-1}$ in the dry state. However, for OECT measurements, P3MEEMT exhibits a reported hole mobility of 6 x 10^{-2} $cm^2 \bullet V^{-1} \bullet s^{-1}$ in the hydrated state.[79] Using values extracted from previous work [101], the OFET μ extracted from P3HT, PTCOOR, and PTCOOH were 1.8 x 10^{-4} ± 7E-5 $cm^2 \bullet V^{-1} \bullet s^{-1}$, 1.2 x 10^{-2} ± 6E-3 $cm^2 \bullet V^{-1} \bullet s^{-1}$, and 2.3 x 10^{-2} ± 8E-3 $cm^2 \bullet V^{-1} \bullet s^{-1}$. For PTOH the extracted OFET mobility was 6.9 x 10^{-3} $cm^2 \bullet V^{-1} \bullet s^{-1}$. It is clear that P3HT, PTCOOR, P3MEEMT, and PTOH swell by at least 10-100x from dry to wet state. This is attributed to hydration of the polymer matrix resulting in faster anion injection rates. PTCOOH remains relatively the same either in wet or solid state. The importance of functionality that is incorporated in the side-chain has major implications on the mixed conduction properties and is clearly demonstrated.

3 Conclusion

This study was aimed at improving the understanding of the relationship between polythiophene OECT properties and their engineered side chains with varied counterions of potassium salt electrolytes. In addition, mixed blends were investigated to evaluate any synergistic effects between functionalities. It is observed that depending on the functional moiety that is attached, a large shift to lower potentials of V_{th}, an increase in drain current, and increase in transconductance are observed for P3HT and PTCOOR, with P3MEEMT. A newly designed and synthesized polymer PTOH was also tested and displayed stability to large shifts in V_{TH}, slight increase in drain current, and little or no increase in transconductance when an ionic radius of the dopant is increased until a much larger anion, large polarizability, and low hydration number such as $TSFI^-$ is used that finally generates an interaction. PTCOOH on the other hand has the same magnitude in shift with respect to any anion that is larger than Cl^-.

The anionic doping process was studied through cyclic voltammetry. Both PTOH and PTCOOH display irreversible undoping/doping ratio which implies that self-doping of the chains must be interfering with the involvement of injecting into the polymer, until a very large sized anion is used. This work demonstrates that side-chain engineering can have substantial difference in the level of interaction in the electrolyte which would require tailoring the ion for specific polymer interactions. As new OECT polymeric materials are developed, it is imperative to study these polymers in different electrolyte settings for applicability purposes and understanding of side chain influence.

4 Methods

Materials and Characterization Techniques

Unless otherwise specified, all chemicals were used as purchased without further purification. Solvents used for workups and cleaning were reagent grade and used as received. All reagents, monomer and polymer synthesis are outlined in the Supporting Information.

Sample Preparation:

For PTCOOR, P3HT, and P3MEEMT all polymers were dissolved at a concentration of 10 mg/ml in anhydrous dichlorobenzene, sonicated for 1 hour, and heated at 60°C for 1 hour. Solutions were cooled to room temperature, filtered with a hydrophobic filter (0.45 μm), and then spincoated onto interdigitated electrodes at 1600 rpm for 60 seconds. Subsequent annealing was performed under high vacuum at 60°C. PTCOOH and PTOH were dissolved at a concentration of 10 mg/ml in anhydrous dimethylformamide, sonicated for 1 hour, heated at 60°C for 1 hour, and heated at 130°C for 20 minutes. The solutions were cooled to room temperature, filtered with a hydrophilic filter (0.45 μm), and then spin-coated onto interdigitated electrodes at 1600 rpm for 320 seconds.[101] For mixed blends, polymers were followed above, however, once filtered the polymers were then mixed 50/50 by volumetric ratio. For PTCOOR and P3MEEMT, the polymers were dissolved in DMF when mixing with either PTOH or PTCOOH to prevent phase segregation or crashing out of solution of polymers due to incompatibility in solvent blend.

OECT Devices. OECTs were purchased from NanoSPR, consisting of an interdigitated electrode array on sital with 150 nm Au layer and 10 μm interdigital gap. The size of the support is 28 mm x 5 mm x 0.4 mm. The length is 1 mm, and width of the finger is 20 μm for all electrode models. The sital gap is 10 μm and the number of interdigit pairs is 20 (40 total added by each side). The area of the system is 1.25 mm^2. The W/L ratio calculated and validated by NanoSPR is 2000. The source-drain bias/current was measured using a KeySight B1500A semiconductor device parameter analyzer. Before use, the electrodes were sonicated in isopropanol for 15 minutes, dried with N_2 , and subjected to UV-ozone treatment for 20 minutes using a Jelight model 18.

Volumetric Capacitance Derivation.

$C_p = \frac{Q}{m*\Delta V}$;

C_p is defined as the specific capacitance (F/g), m (g) is the mass of the active material, Q (Coulombs) is the average of the charges generated from charging and discharging, and ΔV is the potential window that is scanned. Q is also represented as current (I) multiplied by time (t), so a new equation is generated:

$C_p = \frac{I\ x\ t}{m*\Delta V}$;

Rearrangement of the equation provides the new equation (1) defined as:

$I = C_p \bullet m \bullet (\frac{V}{t})$; (Equation 1)

In a CV experiment, the current changes by changing the potential from V_1 to V_2. Therefore, we can rewrite Equation 1 in its integral form:

$$\int_{V1}^{V2} I\ (v)dv = \int_{V1}^{V2} Cp * m * (\frac{V}{t})dv$$

The integral $\int_{V1}^{V2} I\ (v)dv$ = the area A under the CV curve. Therefore:

$$A = \int_{V1}^{V2} Cp * m * (\frac{V}{t})dv$$

UV-vis Absorption Spectroscopy. Absorption spectra were obtained using a Lambda 950 UV-vis spectrometer with an operating range of 175-3300 nm. A universal reflectance accessory was used to measure thin film characterization. Polymers were spin-coated by method outlined above on borosilicate glass slides.

Profilometer. A Filmetrics F20-NIR thin film analyzer was used to measure the thickness of the spincoated polymers on the OECTs. All polymers had thin films ranging from 250-350 ± 50 nm of film thickness when spin-coated.

Differential Scanning Calorimetry (DSC). DSC measurements, using 2-3 mg of material, were conducted under nitrogen scan rate of 10°C/ min when heating and 20°C/min for cooling with a TA DSC-Q20 instrument.

X-ray Diffraction (XRD). Polymers were dissolved in appropriate solvents noted above and drop-cast on Si/SiO_2 (300 nm of thermal oxide growth) substrate to form at least 100 nm of film thickness. The thin films were then collected and analyzed using a Bruker D8 Focus X-ray Diffractometer analyzer. Quantitative analysis was performed with a DIFFRAC^{plus} Software

utilizing DIFFRAC^{plus} EVA and TOPAS programs. Measurements provided intensity distribution related to the angle 2θ. The instrument was calibrated with a NIST standard reference piece of polystyrene or Al_2O_3.

Cyclic Voltammetry. Cyclic voltammetry (CV) measurements were performed in a one-chamber, three-electrode cell using a PGSTAT302 potentiostat. A 2 mm^2 Pt electrode from BASi was used as the working electrode with a platinum wire serving as the counter electrode relative to a Ag/AgCl (nonaqueous) reference electrode submerged in either 0.01 M $AgNO_3$/0.1 M n-Bu_4PF_6 in anhydrous acetonitrile or 0.01 M $AgNO_3$/0.1 M n-Bu_4Cl in anhydrous acetonitrile (MeCN). Measurements were taken in either 0.1 M n-Bu_4PF_6 (in MeCN) electrolyte solution or 0.1 M n-Bu_4Cl (in MeCN) at various scan rate from 10 mV/s to 250 mV/s. Potentials relative to the Ag/Ag^+ couple to which the Fc/Fc^+ couple was measured to be 262 mV (Figure S17 in Supporting Information). The potential for ferrocene redox is -4.8 eV relative to vacuum. Energy levels of the highest occupied molecular orbital (HOMO) were calculated according to the equations:

HOMO = -e(E_{ox}+ 4.64) (eV), where E_{ox} is the onset oxidation potential vs Ag/AgCl.

^{1}H NMR. Spectra were measured on a Bruker Avance 300 MHz Spectrometer and chemical shifts are reported in parts per million (ppm). Spectra were recorded in either $CDCl_3$ or DMSO-d6. **Gel permeation chromatography (GPC)** analysis to determine molecular weight (SI S30-33). The analysis was performed on a Tosoh Bioscience EcoSEC GPC workstation using THF as the eluent (0.35 mL min-1), 40°C through a TSKgel SuperMultipore HZ-M guard column (4.6 mm ID x 2.0 cm, 4 mm, Tosoh Bioscience). Polystyrene standard (EasiVial PS-M, Agilent) was used to build a

calibration curve. Polymers were dissolved in THF (2 mg mL-1), filtered (Millex-FG Syringe Filter Unit, 0.20 mm, PTFE, EMD Millipore) and injected using an auto-sampler (10 μL). PTCOOH and PTCOOR were purchased from Rieke Metals with a reported molecular weight average of 15,000-25,000. PTOH was insoluble in THF when protecting group was cleaved to form hydroxyl terminated ends; therefore, PTOTBS will be used as the reported value.

OECT Measurements. Measurements were conducted using a KeySight 1500 Semiconductor Device Analyzer. Transfer curves were obtained by measuring the V_g from 0 V to -1 V with a step size of -10 mV and V_D = -0.6 V. Output curves were measured from 100 mV to -1 V with a step size of -11 mV, and V_g ranged from 0 V to -700 mV with a step size of -50 mV. However, for polymers like P3MEEMT and P3HT, V_g ranged from -600 mV to -1.05 V with a step size of -50 mV with KCl. Afterwards, the original setup listed before was used. The reference electrode that was used was a Ag/AgCl (sat'd KCl) purchased from GAMRY instruments. The Electrode potential is 199 mV vs Normal Hydrogen Electrode (NHE).

Scanning Electron Microscopy (SEM). Measurements were conducted by drop-casting polymer ink solutions outlined in the sample preparation on microscope glass slide (borosilicate). A Tescan Mira 3 GMU field emission gun SEM with EDAX was used to determine the film thickness of drop-casted films prepared on platinum electrodes that were used for cyclic voltammetry studies. Film thickness ranged from 1-10 μm.

Acknowledgements. Principal support of this work was by the National Science Foundation, Division of Materials Research, Biomaterials Program, Grant No. 1807292. Participation of Taein Lee was supported by the National Science Foundation DMREF program, Grant No. 1728947. The authors thank Professor Rebekka Klausen (Johns Hopkins University) and Yuyang Ji for use of the GPC facility; Soumyodip Banerjee in Professor Sara Thoi's group for electrochemistry consultation; Professor J.D. Tovar and Nicholas Adams for potentiostat use for cyclic voltammetry results and electrolyte preparation; Johndavid Sabedra and Professor Tyrel McQueen for XRD use and experimental assistance, and Dr Tushita Mukhopadhyaya for valuable discussions.

5 References

1) Pankow, R.M.; Thompson. B.C. The Development of Conjugated Polymers as the Cornerstone of Organic Electronics. *Polymer*. **2020**, 207, 122874. https://doi.org/10.1016/j.polymer.2020.122874
2) Søndergaard, R.R.; Hösel, M.; Krebs, F.C. Roll-to-Roll Fabrication of Large Area Functional Organic Materials. *J. Polym. Sci. B Polym. Phys*., **2013**, 51, 16-34. https://doi.org/10.1002/polb23192.
3) Forrest, S.R. The Path to Ubiquitous and Low-Cost Organic Electronic Appliances on Plastic. *Nature*. **2004**, 428. 911-918. https://doi.org/10.1038/nature02498
4) Mei, J.; Bao, Z**.** Side Chain Engineering in Solution Processable Conjugated polymers. *Chem. Mater*. **2014**, 26 (1), 604-615. https://doi.org/10.1021/cm4020805
5) Dai, L.; Winkler, B.; Dong, L.; Tong, L.; Mau, A.W.H. Conjugated Polymers for Light-Emitting Applications. *Adv. Mater*. **2001**, 13 (12-13). 915-925. https://doi.org/10.1002/1521-4095(200107)13:12/13<915::AID-ADMA915>3.0.CO;2-N

6) Yu, D.X. Light-Emitting Devices with Conjugated Polymers. *Int J Mol Sci*. **2011**, 12(3): 1575-1594. https://doi.org/ 10.3390/ijms12031575

7) AlSalhi, M.S.; Alam, J.; Dass, L.A.; Raja, M. Recent Advances in Conjugated Polymers for Light Emitting Devices. *Int. J. Mol. Sci*. **2011**, 12 (3), 2036-2054. https://doi.org/10.3390/ijms12032036

8) Grimsdale, A.C.; Chan, K.L.; Martin, R.E.; Jokisz, P.G.; Holmes, A.B. Synthesis of Light-Emitting Conjugated Polymers for Applications in Electroluminescent Devices. *Chem. Rev*. **2009**, 109 (3), 897-1091. https://doi.org/10.1021/cr000013v

9) Yang, J.; Zhao, Z.; Wang, S.; Guo, Y.; Liu, Y. Insight Into High-Performance Conjugated Polymers for Organic Field-Effect Transistors. *Chem.* **2018**, 4 (12), 2748-2785. https://doi.org/10.1016/j.chempr.2018.08.005

10) Kimpel, J.; Michinobu, T. Conjugated Polymers for Functional Applications: Lifetime and Performance of Polymeric Organic Semiconductors in Organic Field-Effect Transistors. *Polym In*. **2021**; 70: 367-373 https://doi.org/10.1002/pi.6020

11) Ashizawa, M.; Zheng, Y.; Tran, H.; Bao, Z. Intrinsically Stretchable Conjugated Polymer Semiconductors in Field Effect Transistors. *Progress in Polymer Science*, **2020**, 100, 101181. https://doi.org/10.1016/j.progpolymsci.2019.101181

12) Wang, C.; Dong, H.; Hu, W.; Liu, Y.; Zhu, D. Semiconducting π-Conjugated Systems in Field-Effect Transistors: A Material Odyssey of Organic Electronics. *Chem Rev*. **2012**, 112, 2208-2276. https://doi.org/10.1021/cr100380z

13) Acchetti, A. π-Conjugated Polymers for Organic Electronics and Photovoltaic Cell Applications. *Chem. Mater*. **2011**, 23 (3), 733-758. https://doi.org/10.1021/cm102419z

14) Coakley, K.M.; McGehee, M.D. Conjugated Polymer Photovoltaic Cells. *Chem. Mater*. **2004**, 16 (23), 4533-4542. Chem. Mater. 2004, 16 (23), 4533-4542. https://doi.org/10.1021/cm049654n

15) Mozer, A.J.; Sariciftci, S. Conjugated Polymer Photovoltaic Devices and Materials. *Comptes Rendus Chimie*. **2006**, 9 (5-6), 568-577. https://doi.org/10.1016/j.crci.2005.03.033

16) Chen, J.T.; Hsu, C.S. Conjugated Polymer Nanostructures for Organic Solar Cell Applications. *Polym. Chem*. **2011**, 2, 2707-2722. https://doi.org/10.1039/C1PY00275A

17) Zeglio, E.; Inganäs, O. Active Materials for Organic Electrochemical Transistors. *Adv. Mater*. **2018**, 30, 1800941. https://doi.org/10.1002/adma.201800941

18) Rahman, M.A.; Kumar, P.; Park, D.S.; Shim, Y.B. Electrochemical Sensors Based on Organic Conjugated Polymers. *Sensors*. **2008**, 8 (1): 118-141. https://doi.org/10.3390/s8010118.

19) Wang, D.; Gong, X.; Heeger, P.S.; Rininsland, R.; Bazan, G.C.; Heeger, A.J. Biosensors from Conjugated Polyelectrolyte Complexes. *PNAS*. **2002**, 99 (1), 49-53. https://doi.org/10.1073/pnas.012581399.

20) Hui, X.; Haiping, W.; Chunhai, F.; Wenxin, L.; Zhizhou, Z.; Lin, H. Highly Sensitive Biosensors Based on Water-Soluble Conjugated Polymers. *Chinese Science Bulletin*. **2004**, 49, 2227-2231. https://doi.org/10.1360/982004-33.

21) Yun, M.; Yan, Z.; Wenqui, D.; Zhihu, M.; Zhengjian, Q. The Application of DNA Biosensor Based on Conjugated Polymers. *Progress in Chemistry*. **2015**. 27 (12): 1799-1807. https://doi.org/10.7536/PC150636

22) Traina, C.A.; Bakua, Rc 2nd; Bazan, G.C. Design and Synthesis of Monofunctionalized, Water-Soluble Conjugated Polymers for Biosensing and Imaging Applications. *Journal of the American Chemical Society*. **2011**, 133 (32): 12600-12607. https://doi.org/10.1021/ja202877q

23) Palza, H.; Zapata, P.A.; Angulo-Pineda, C. Electroactive Smart Polymers for Biomedical Applications. *Materials*. **2019**, 12, 277 https://doi.org/10.3390/ma12020277.

24) Liu, Y.; Servant, A.; Guy, O.J.; Al-Jamal, K.T.; Williams, P.R.; Hawkins, K.M.; Kostarelos, K. An Electric-Field Responsive Microsystem for Controllable Miniaturized Drug Delivery Applications. *Procedia Engineering*. **2011**, 25, 984-987. https://doi.org/10.1016/j.proeng.2011.12.242.

25) Cabane, E.; Zhang, X.; Langowska, K.; Palivan, C.G.; Meier, W. Stimuli-Responsive Polymers and their Applications in Nanomedicine. *Biointerphases*.**2012**, 7, 9. https://doi.org/10.1007/s13758-011-0009-3

26) Guo, B.; Ma, P.X. Conducting Polymers for Tissue Engineering. *Biomacromolecules*. **2018**, 19 (6): 1764-1782. https://doi.org/10.1021/acs.biomac.8b00276

27) Kohane, D.S.; Langer, R. Polymeric Biomaterials in Tissue Engineering. *Pediatric Research*. **2008**. 63 (5), 487-491. https://doi.org/10.1203/01.pdr.0000305937.26105.e7

28) Higgins, S.G.; lo Fiego, A.; Patrick, L.; Creamer, A.; Stevens, M.M. Organic Bioelectronics: Using Highly Conjugated Polymers to Interface with Biomolecules, Cells, and Tissues in the Human Body. *Advanced Materials Technologies*. **2020**, 5 (11). https://doi.org/10.1002/admt.202000384.

29) Park, Y.; Jung, J.; Chang, M. Research Progress on Conducting Polymer-Based Biomedical Applications. *Appl. Sci*. **2019**, 9, 1070. https://doi.org/10.3390/app9061070

30) Roni, R.; Ali, A.; Shavandi, A.; Clarkson, A.N. Current and Novel Polymeric Biomaterials for Neural Tissue Engineering. *Journal of Biomedical Science*. **2018**, 25: 90. https://doi.org/10.1186/s12929-018-0491-8

31) Liu, S.; Chen, X.; Liu, G. Conjugated Polymers for Information Storage and Neuromorphic Computing. *Polymer International*. **2020**, 70 (4), 374-403. https://doi.org/10.1002/pi.6017.

32) van Doremaele, E.R.W.; Gkoupidenis, P.; van de Burgt, Y. Towards Organic Neuromorphic Devices for Adaptive Sensing and Novel Computing Paradigms in Bioelectronics. *J. Mater. Chem. C*., **2019**, 7, 12754. https://doi.org/10.1039/c9tc03247a

33) Lee, Y.; Lee, T.W. Organic Synapses for Neuromorphic Electronics: From Brain -Inspired Computing to Sensorimotor Nervetronics. *Acc. Chem. Res*. **2019**, 52 (4), 964-974. https://doi.org/10.1021/acs.accounts.8b00553

34) Riess, I. Mixed Ionic-Electronic-Conductors-Material Properties and Applications. *Solid State Ionics*. **2003**, 157 (1-4), 1-17. https://doi.org/10.1016/S0167-2738(02)00182-0

35) Paulsen, B.D.; Tybrandt, K.; Stabrinidou, E.; Rivnay, J. Organic-Mixed Ionic-Electronic Conductors. *Nature Materials*. **2020**, 19, 13-26. https://doi.org/10.1038/s41563-019-0435-z

36) Riess, I. Potentiometric Sensors Based on Mixed Ionic-Electronic Conductors Instead of Solid Electrolytes. *Solid State Ionics*. **1992**. 51 (1-2), 109-114. https://doi.org/10.1016/0167-2738(92)90352-P

37) Liu, Y.; Ogawa, K.; Schanze, K.S. Conjugated Polyelectrolytes as Fluorescent Sensors. *Photochemistry Review*. **2009**, 10 (4), 173-190. https://doi.org/10.1016/j.jphotochemrev.2009.10.003.

38) Cui, B.; Liu, P.; Liu, X.; Liu, S.; Zhang, Z. Molecularly Imprinted Polymers for Electrochemical Detection and Analysis: Progress and Perspectives. *Journal of Materials Research and Technology*. **2020**. 9(6), 12568-12584. https://doi.org/10.1016/j.jmrt.2020.08.052.

39) Morichetti, F.; Zanotto, S.; Blancato, A.; Berkemeier, F.; Castro, M.M.; Buchheit, A.; Wiemhöfer, H.D.; Schmitz, G. Electrochemical Optical Actuators: Controlling the Light Through Ions," *2016 18th International Conference on Transparent Optical Networks (ICTON)*, **2016**, pp. 1-4, doi: 10.1109/ICTON.2016.7550296

40) Savva, A.; Hallani, R.; Cendra, C.; Surgalis, J.; Hidalgo, T.C.; Wusoni, S.; Sheelamanthula, R.; Chen, X.; Kirkus, M.; Giovannitti, A.; Salleo, A.; McCulloch, I.; Inal, S. Balancing Ionic and Electronic Conduction for High-Performance Organic Electrochemical Transistors. *Advanced Functional Materials*. **2020**. 30 (11). 1907657. https://doi.org/10.1002/adfm.201907657

41) Tu, D.; Fabiano, S. Mixed Ion-Electron Transport in Organic Electrochemical Transistors. *Appl. Phys. Lett*. **2020**, 117, 080501. https://doi.org/10.1063/5.0012599

42) Inal, S.; Malliara, G.G.; Rivnay, J. Mixed Ion-Electron Transport in Organic Electrochemical Transistors. *Appl. Phys. Lett*. **2020**, 117, 080501. https://doi.org/10.1063/5.0012599

43) Inal, S.; Malliara, G.G.; Rivnay, J. Benchmarking Organic Mixed Conductors for Transistors. *Nature Communications*. **2017**, 8, 1767. https://doi.org/10.1038/s41467-017-01812-w.

44) Friedlein, J.T.; Rivnay, J. Device Physics of Organic Electrochemical Transistors. *Organic Electronics*. **2018**, 63, 398-414. https://doi.org/10.1016/j.orgel.2018.09.0101.

45) Nissa, J.; Janson, P.; Simon, D.T.; Berggren, M. Expanding the Understanding of Organic Electrochemical Transistor Function. *Appl. Phys. Lett*. **2021**, 118, 053301. https://doi.org/10.1063/5.0039345

46) Giovannitti, A.; Nielsen, C.B.; Sbircea, D.T.; Inal, S.; Donahue, M.; Niazi, M.R.; Hanifi, D.A.; Amassian, A.; Malliara, G.G.; Rivnay, J.; McCulloch, I. N-type Organic Electrochemical

Transistors with Stability in Water. *Nature Communications*. **2016**, 7, 13066. https://doi.org/10.1038/ncomms13066

47) Rivnay, J.; Leleux, P.; Ferro, M.; Sessolo, M.; Williamson, A.; Koutsouras, D.A.; Khodagholy, D.; Ramuz, M.; Strakosas, X.; Owens, R.M.; Benar, C.; Badier, J.M.; Bernard, C.; Malliaras, G.High Performance Transistors for Bioelectronics Through Tuning of Channel Thickness. *Science Advances*. **2015**, 1 (4), e1400251. https://doi.org/10.1126/sciadv.1400251

48) Wu, X.; Liu, Q.; Surendran, A.; Bottle, S.E.; Sonar, P.; Leong, W.L. Enhancing the Electrochemical Doping Efficiency in Diketopyrrolopyrrole-Based Polymer for Organic Electrochemical Transistors. *Adv. Electron Mater*. **2021**, 7, 7, 2000701 https://doi.org.10.1002/aelm.202000701

49) Kim, S.M.; Kim, C.H.; Kim, Y.; Kim, N.; Lee, W.J.; Lee, E.H.; Kim, D.; Park, S.; Lee, K.; Rivnay, J.; Yoon, M.H. Influence of PEDOT:PSS Crystallinity and Composition on Electrochemical Transistor Performance and Long-Term Stability. *Nature Communications*. **2018**, 9, 3858. https://doi.org/10.1038/s41467-018-06084-6

50) Keene, S.T.; van der Pol, T.P.A.; Zakhidov, D.; Weijtens, H.L.; Janssen, R.A.J.; Salleo, A.; van de Burgt, Y. Enhancement-Mode PEDOT:PSS Organic Electrochemical Transistors using Molecular De-Doping. *Advanced Materials*. **2020**, 32 (19), 2000270. https://doi.org/101002/adma.202000270

51) Tan, K.; Miao, W.; Guo, S. Crosslinked PEDOT: PSS Organic Electrochemical Transistors on Interdigitated Electrodes with Improved Stability. *ACS Appl Polym. Mater*. **2021**, 3 (3), 1436-1444. https://doi.org/10.1021/acsapm.0c01292

52) Flagg, L.Q.; Bischak, C.G.; Onorato, J.W.; Rashid, R.B.; Luscombe, C.K.; Ginger, D.S. Polymer Crystallinity Controls Water Uptake in Glycol Side Chain Polymer Organic Electrochemical Transistors. *J. Am. Chem. Soc*. **2019**, 141, 4345−4354. https://doi.org/10.1021/jacs.8b12640

53) Flagg, L.Q.; Giridharagopal, R.; Guo, J.; Ginger, D. S. Anion- Dependent Doping and Charge Transport in Organic Electrochemical Transistors. *Chem. Mater*. **2018**, 30, 5380−5389. https://doi.org/10.1021/acs.chemmater.8b02220

54) Savva, A.; Cendra, C.; Giugni, A.; Torre, B.; Surgailis, J.; Ohayon, D.; Giovannitti, A.; McCulloch, I.; Fabrizio, E.D.; Salleo, A.; Rivnay, J.; Inal, S. Influence of Water on the Performance of Organic Electrochemical Transistors. *Chem. Mater*. **2019**, 31 (3), 927-937. https://doi.org/10.1021/acs.chemmater.8b04335

55) Moser, M.; Hidalog, T.; Surgailis, J.; Gladisch, J.; Ghosh, S. Sheelamanthula, R.; Thiburce, Q.; Giovannitti, A.; Salleo, A.; Gasparini, N.; Wadsworth, A.; Zozoulenko, I.; Berggren, M.; Starinidou, E.; Inal, S.; McCulloh, I. Side Chain Redistribtuion as a Strategy to Boost Organic Electrochemical Transistor Performance and Stability. *Adv. Mater*. **2020**, 32, 20002748. https://doi.org/10.1002/adma.202002748

56) Moser, Savagian, L.R.; Savva, A.; Matta, M.; Ponder Jr., J.F.; Hidalgo, T.C.; Ohayon, D.; Hallani, R.; Reisialali, M.; Troisi, A.; Wadsworth, A.; Reynolds, J.R.; Inal, S.; McCulloch, I. Ethylene Glycol-Based Side Chain Length Engineering in Polythiophenes and its Impact on Organic Electrochemical Transistor Performance. *Chem. Mater*. **2002**, 32, 6618-6628. https://doi.org/10.1021/acs.chemmater.0c02041.

57) Bischak, C.G.; Flagg, L. Q.; Yan, K.; Rehman, T.; Davies, D.W.; Quezada, R.J.; Onorato, J.W.; Luscombe, C.K.; Diao, Y.; Li, C.Z.; Ginger, D.S. A Reversible Structural Phase Transistion by

Electrochemically Driven Ion Injection into a Conjugated Polymer. *J. Am. Chem. Soc*. **2020**, 142, 7434-7442. https://doi.org/10.1021/jacs.9b12769

58) Giovannitti, A.; Sbircea, D.T.; Inal, S.; Nielsen, C.B.; Bandiello, E.; Hanifi, D.A.; Sessolo, M.; Malliaras, G.G.; McCulloch, I.; Rivnay, J. Controlling the Mode of Operation of Organic Transistors Through Side-Chain Engineering. *Proc Natl Acad Sci USA*. **2016**, 113 (43): 12017-12022. https://doi.org/10.1073/pnas.1608780113.

59) Giovannitti, A.; Maria, I.P.; Hanifi, D.; Donahue, M.J.; Bryant, D.; Barth, K.J.; Makdah, B.E.; Savva, A.; Moia, D.; Zetek, M.; Barnes, P.R.F.; Reid, O.G.; Inal, S.; Rumbles, G.; Malliaras, G.G.; Nelson, J.; Rivnay, J. McCulloch, I. The Role of the Side Chain on the Performance of N-type Conjugated Polymers in Aqueous Electrolytes. *Chem. Mater.* **2018**, *30*, 2945. https://doi.org/10.1021/acs.chemmater.8b00321

60) Khau, B.; Savagian, L.R.; Keersmaecker, M.D.; Gonzalez, M.A.; Reichmanis, E. Carboxylic Acid Functionalization Yields Solvent-Resistant Organic Electrochemical Transistors. *ACS Materials Lett*. **2019**, 1, 599-605. https://doi.org/10.1021/acsmaterialslett.9b00373

61) Bischak, C.G.; Flagg, L.Q.; Ginger, D.S. Ion Exchange Gels Allow Organic Electrochemical Transistor Operation with Hydrophobic Polymers in Aqueous Solution. *Adv. Mater*. **2020**, 32, 2002610. https://doi.org/10.1002/adma.202002610

62) Tan, S.T.M.; Keene, S.; Giovannitti, A.; Melianas, A.; Moser, M.; McCulloch, I.; Salleo, A. Operation Mechanism of Organic Electrochemical Transistors as Redox Chemical Transducers. *ChemRxiv*. **Preprint**. https://doi.org/10.2634/chemrxiv.14545945.v1

63) Kumar, P.; Yi, Z.; Zhang, S.; Sekar, A.; Soavi, F.; Cicoira, F. Effect of Channel Thickness Electrolyte Ions, and Dissolved Oxygen on the Performance of Organic Electrochemical Transistors. *Appl. Phys. Lett*. **2015**. 107, 053303. https://doi.org/10.1063/1.4927595

64) Wu, X.; Surendran, A.; Ko, J.; Filonik, O.; Herzig, E.M.; Müller-Buschbaum, P.; Leong, W.L. Ionic-Liquid Doping Enables High Transconductance, Fast Response Time, and High Ion Sensitivity in Organic Electrochemical Transistors. *Advanced Materials*. **2018**, 31 (2), 1805544. https://doi.org/10.1002/adma.201805544

65) Dong, B.X.; Nowak, C.; Onorato, W.; Strzalka, J.; Escobedo, F.A.; Luscombe, C.K.; Nealey, P.F.; Patel, S.N. Influence of Side-Chain Chemistry on Structure and Ionic Conduction Characteristics of Polythiophene Derivatives: a Computational and Experimental Study. *Chem. Mater*. **2019**, 31, 1418-1429. https://doi.org/10.1021/acs.chemmater.8b05257

66) Khau, B.V.; Scholz, A.D.; Reichmanis, E. Advances and Opportunities in Development of Deformable Organic Electrochemical Transistors. *Journal of Materials Chemistry, C*. **2020**, 8, 15067-15078. https://doi.org/10.1039/D0TC03118F.

67) Stefan, M.C.; Bhatt, M.P.; Sista, P.; Magurudeniva, H.D. Grignard Metathesis (GRIM) Polymerization for the Synthesis of Conjugated Block Copolymers Containing Regioregular Poly(3-hexylthiophene). *Polym. Chem*. **2012**, 3, 1693-1701. https://doi.org/10.1039/C1PY00453K

68) Stefan, M.C.; Javier, A.E.; Osaka, I.; McCullough, R.D. Grignard Metathesis Method (GRIM): Toward a Universal Method for the Synthesis of Conjugated Polymers. *Macromolecules*. **2009**. 42 (1), 30-32. https://doi.org/10.1021/ma8020823.

69) Kiriy, A.; Senkovskvy, Sommer, M. Kumada Catalyst-Transfer Polycondensation: Mechanism, Opportunities, and Challenges. *Macromol. Rapid Commun*. **2011**, 32, 1503-1517. https://doi.org/10.1002/marc.201100316

70) Sahalianov, I.; Hynynen, J.; Barlow, S.; Marder, S.R.; Müller, C.; Zozoulenko, I. UV-to-IR Absorption of Molecularly p-Doped Polythiophenes with Alkyl and Oligoether Side-Chains: Experiment and Interpretation Based on Density Functional Theory. *J. Phys. Chem. B*. **2020**, 124, 49, 11280-11293. https://doi.org/10.1021/acs.jpcb.0c08757

71) Finn, P.A.; Jacobs, I.E.; Armitage, J.; Wu, R.; Paulsen, B.D.; Freeley, M.; Palma, M.; Rivnay, J.; Sirringhaus, H.; Nieslen, C. Effect of Polar Side Chains on Neutral and P-Doped Polythiophene. *J. Mater. Chem. C*. **2020**, 8, 16216-16223 https://doi.org/10.1039/D0TC04290K.

72) Rahimi, K.; Botiz, I.; Agumba, J.O.; Motamen, S.; Stingelin, N.; Reiter, G. Light Absorption of Poly(3-hexylthiophene) Singe Crystals. *RSC Adv*. **2014**, 4, 1121-11123. https://doi.org/10.1039/C3RA47064D

73) Clark, J.; Chang, J.F.; Spano, F.C.; Friend, R.H.; Silva, C. Determining Exciton Bandwidth and Film Microstructure in Polythiophene Films Using Linear Absorption Spectroscopy. *Appl. Phys. Lett*. **2009**, 94, 163306. https://doi.org/10.1063/1.3110904.

74) Spano, F.C.; Silva, C. H- and J- Aggregate Behavior in Polymeric Semiconductors. *Annu Rev Phys Chem*. **2014**, 65, 477-500. https://doi.org/10.1146/annurev-physchem-040513-103639.

75) Amarasekara, A.S.; Pomerantz, M. Synthesis and Study of Head-to-Tail Regioregular Poly(Alkyl Thiophene-3-Carboxylates). *Synthesis*. **2003**, 14: 2255-2258. https://doi.org/10.1055/s-2003-41495.

76) Zhou, C.Y.; Yan, L.T.; Zhang, L.N.; Ai, X.D.; Li, T.X.; Dai, C.A. Synthesis of Regioregular 3-Carboxylic Ester Substituted Polythiophene and its Copolymer with Thiophene. *Journal of Macromolecular Science, Part A*. **2012**, 49 (4): 293-297. https://doi.org/10.1080/10601325.2012.662037

77) Kim, H.C.; Kim, J.S.; Baek, S.; Ree, M. Functional Polythiophene Bearing Hydroxyethyl Groups and their Derivatives. *Macromolecular Research*. **2006**. 14 (2), 173-178. https://doi.org/10.1007/BF03218505

78) Bilger, D.W.; Figueroa, J.A.; Redeker, N.D.; Sarkar, A.; Stefik, M.; Zhang, S. Hydrogen-Bonding-Directed Ordered Assembly of Carboxylated Poly(3-Alkylthiophene)s. *ACS Omega*. **2017**, 2, 8526-8535. https://doi.org/10.1021/acsomega.7b01361.

79) Schmode, P. Savva, A.; Kahl, R.; Ohayon, D.; Meischsner, F.; Dolynchuk, O. The Key Role of Side Chain Linkage in Structure Formation and Mixed Conduction of Ethylene Glycol Substituted Polythiophenes. *ACS Applied Materials & Interfaces*. **2020**. 12 (11), 13029-13039. https//doi.org/10.1021/acsami.9b21604

80) El-Sayed, M.; Müller, H.; Rheinwald, G.; Lang, H.; Spange, S. UV/Vis Spectroscopic Properties of N-(2'-Hydroxy-4'-N,N-dimethyl-aminobenzylidene)-4-Nitroaniline in Various Solvents and Solid Environments. *Monatshefte für Chemie*. **2003**, 134, 361-370. https://doi.org/10.1007/s00706-002-0550-3.

81) Nieuwendaal, R.C.; Snyder, C.R.; de Longchamp, D.M. Measuring Order in Regioregular Poly(3-hexylthiophene) with Solid-State 13C CPMAS NMR. *ACS Macro Lett.* **2014**, 3, 130-135. https://doi.org/10.1021/mz4005343.

82) Kazarinoff, P.D.; Shamburger, P.J.; Ohuchi, F.S.; Luscombe, C.K. OTFT performance of Air-Stable Ester-Functionalized Polythiophenes. *J. Mater. Chem*. **2010** 20, 3040-3045. https://doi.org/10.1039/B927164C

83) Ong, B.S.; Wu, Y.; Liu, P.; Gardner, S. High-Performance Semiconducting Polythiophenes for Organic Thin-Film Transistors. *J. Am. Chem. Soc*. **2004**, 126, 11, 3378-3379. https://doi.org/10.1021/ja039772w

84) Ishay, R.B.; Harel, Y.; Lavi, R.; Lellouche, J.P. Multiple Functionalization of Tungsten Disulfide Inorganic Nanotubes by Covalently Grafted Conductive Polythiophenes. *RSC Advances*. **2016**. 92 (6), 89585-89598. https://doi.org/10.1039/C6RA19628D

85) Fei, Z.; Boufflet, P.; Wood, S.; Wade, J.; Moriarty, J.; Gann, E.; Ratcliff, E.L.; McNeilll, C.R.; Sirringhaus, Kim, J.S.; Heeney, M. Influence of Backbone Fluorination in Regioregular Poly (3-alkyl-4-fluoro)thiophenes. *J. Am. Chem. Soc*. **2015**, 137, 6866-6879. https://doi.org/10.1021/jacs.5b02785

86) Remy, R.; Weiss, E.D.; Nguygen, N.A.; Wei, S.; Campos, L.M.; Kowalewski, T.; Mackay, M.E. Enthalpy of Fusion of Poly(3-hexylthiophene) by Differential Scanning Calorimetry. *J. Polym. Sci., Part B: Polym. Phys*. **2014**, 52, 1469-1475. https://doi.org/10.1002/polb.23584.

87) Dong, B.X.; Nowak, C.; Onorato, J.W.; Strzalka, J.; Escobedo, F.A.; Luscombe, C.K.; Nealey, P.F.; Patel, S.N. Influence of Side-Chain Chemistry on Structure on Structure and Ionic Conduction Characteristics of Polythiophene Derivatives: a Computation and Experimental Study. *Chem. Mater*. **2019**, 31, 4, 1418-1429. https://doi.org/10.1021/acs.chemmater.8b05257

88) Mescoloto, A.d.F.; Pulcinelli, S.H.; Santilli, C.V.; Gonçalves, V.C. Structural and Thermal Properties of Carboxylic Acid Functionalized Polythiophenes. *Polímeros*. **2014**, vol 24, 31-35.. https://doi.org/10.4322/polimeros.2014.049

89) Matta, M.; Wu, R.; Paulsen, B.D.; Petty, A.; Sheelamanthula, R.; McCulloch, I.; Schatz, G.C.; Rivnay, J. Ion Coordination and Chelation in a Glycolated Polymer Semiconductor: Molecular Dyanmics and X-Ray Fluorescence Study. *Chem. Mater*. **2020**, 32, 17, 7301-7308. https://doi.org/10.1021/acs.chemmater.0c01984

90) Kim, C.H.; Castro-Carranza, A.; Estrada, M.; Cerdeira, A.; Vonnassieux, Y.; Horowitz, G.; Iñiguez, B. A Compact Model for Organic Field-Effect Transistors with Improved Output Asymptotic Behaviors. *IEEE Transactions on Electron Devices*. **2013**, 60 (3), 1136-1141. https://doi.org/10.1109/TED.2013.2238676

91) Zhang, Y.; Cao, K. Zhu, X.; Li, X.; Qiao, X.; Gu, G.; Zhang, B.; Huang, D.; Shen, Y.; Wang, M. Effect of the Molecular Weight of Poly(3-hexylthiophene) on the Performance of Solid-State Dye-Sensitized Solar Cells. *RSC Advances*. **2013**, 3, 14037. https://doi.org/10.1039/C3RA4138E.

92) Harris, J.K.; Ratcliff, E.L. Ion Diffusion Coefficients in Poly(3-Alkylthiophenes) for Energy Conversion and Biosensing: Role of Side-Chain Length and Microstructure. *J. Mater. Chem. C*. **2020**, 8, 13319-13327. https://doi.org/ 10.1039/D0T03690K.

93) Skompska, M.; Szkurlat, A. The Influence of the Structural Defects and Microscopic Aggregation of Poly(3-alkylthiophenes) on Electrochemical and Optical Properties of the Polymer Films: Discussion of an Origin of Redox Peaks in the Cyclic Voltammograms. *Electrochimica Acta*. **2001**, 46 (26-27), 4007-4015. https://doi.org/10.1016/S0013-4686(01)00710-1

94) Acevedo-Peña, P.; Baray-Calderón, A.; Hu, H.; González, I.; Ugalde-Saldivar, V.M. Measurements of HOMO-LUMO Levels of Poly(3-hexylthiophene) Thin Films by a Simple Electrochemical Method. *Journal of Solid-State Electrochemistry*. **2017**, 21, 2407-2414. https://doi.org/10.1007/s10008-017-3587-2

95) Khylabich, P.P.; Burkhart, B.; Rudenko, A.; Thompson, B.C. Optimization and Simplification of Polymer-Fullerene Solar Cells through Polymer and Active Layer Design. *Polymer*. **2013**. 54 (20), 5267-5298. https://doi.org/10.1016/j.polymer.2013.07.053.

96) Allagui, A.; Freeborn, T.J.; Elwakil, A.S.; Maundy, B.J. Reevaluation of Performance of Electric Double-Layer Capacitors from Constant-Current Charge/Discharge and Cyclic Voltammetry. *Scientific Reports*. **2016**, 6, 38568. https://doi.org/10.1038/srep38568.

97) Jiang, H.; Yang, L.; Li, C.; Yan, C.; Lee, P.S.; Ma, J. High-Rate Electrochemical Capacitors from Highly Graphitic Carbon-Tipped Manganese Oxide/Mesoporous Carbon/Manganese Oxide Hybrid Nanowires. *Energy and Environmental Science*. **2011**, 4, 1813-1819. https://doi.org/10.1039/C1EE01032H.

98) Yu, J.; Fu, N.; Zhao, J.; Liu, R.; Li, F.; Du, Y.; Yang, Z. High specific Capacitance Electrode Material for Supercapacitors Based on Resin-Derived Nitrogen-Doped Porous Carbons. *ACS Omega*. **2019**, 4 (14), 15904-15911. https://doi.org/10.1021/acsomega.9b01916.

99) Romele, P.; Ghittorelli, M.; Kovács-Vajna, Z.M.; Torricelli, F.; Ion Buffering and Interface Charge Enable High Performance Electronics with Organic Electrochemical Transistors. *Nature Communications*. **2019**. 10: 3044. https://doi.org/10.1038/s41467-019-11073-4

100) Duong, D.T.; Tuchman, Y.; Chkthranont, P.; Cavassin, P.; Colucci, R.; Jaramillo, T.F.; Salleo, A.; Faria, G.C. A Universal Platform for Fabricating Organic Electrochemical Devices. *Advanced Electronic Materials*. **2018**. 4 (7), 1800090. https://doi.org/10.1002/aelm.201800090

101) Wagner, J.; Jang, H.J.; Han, J.; Katz, H.E. Enhanced and Unconventional Responses in Chemiresistive Sensing Devices for Nitrogen Dioxide and Ammonia from Carboxylated Alkylthiophene Polymers. *Mater. Horiz*. **2020**, 7, 1358-1371. https://doi.org/10.1039/D0MH00049C